NATIONAL TECHNICAL UNIVERSITY OF ATHENS

CHEMICAL ENGINEERING DEPARTMENT

INTERDISCIPLINARY INTERDEPARTMENTAL POSTGRADUATE PROGRAM –

MATERIAL SCIENCE AND TECHNOLOGY

MASTER'S THESIS

Synthesis of Metal-Organic Frameworks (MOFs) for Electrocatalytic CO_2 Reduction

Magdalini Theologiti

MEng - Chemical Engineering Diploma, University of Patras

Registration Number: 51120009

Supervisor: Christos Argirusis, NTUA Professor

ATHENS, 2022

NATIONAL TECHNICAL UNIVERSITY OF ATHENS

CHEMICAL ENGINEERING DEPARTMENT

INTERDISCIPLINARY INTERDEPARTMENTAL POSTGRADUATE PROGRAM –

MATERIAL SCIENCE AND TECHNOLOGY

MASTER'S THESIS

Synthesis of Metal-Organic Frameworks (MOFs) for Electrocatalytic CO_2 Reduction

Magdalini Theologiti

MEng - Chemical Engineering Diploma, University of Patras

Registration Number: 51120009

SELECTION BOARD:

Christos Argirusis, Professor, Chemical Engineering Department, NTUA

ATHENS, 2022

Acknowledgments

First of all, I would like to express my respect and gratefulness to the professor, Mr. Christos Argirusis, head of the Laboratory of Inorganic Materials and Technology and professor at Chemical Engineering Department in NTUA, for the acceptance, encouragement and help during the conduction of this thesis. Under his guidance and professionality, I was able to broaden my horizons regarding my studies on material synthesis and applications.

Moreover, I would like to thank Christos Vaitsis PhD candidate in Laboratory of Inorganic Materials Technology, for his guidance, support and most of all, patience during the conduction of these experiments. His knowledge and assistance on the matters of MOF synthesis and CO_2 reduction made it possible for me to carry out this thesis

Also, I would like to thank all the members of the LIMT lab for their cooperation and help in times of need during the lab experiments.

Finally, I would like to thank my family and friends for their patience and support. Especially, I would like to express my merit thankfulness to my friends and fellow students, Mrs Christina Aggelara and Mrs Lina Manasi. This thesis would not have been finished without their support.

Abstract

One of the greatest challenges humanity is facing today is the environmental crisis, accompanied by an energy one. The increase of greenhouse gases and the depletion of fuels has turned the scientific interest towards the research of new environmentally friendly and sustainable ways of reversing these problems.

CO_2 reduction is an innovative method of converting this pollutant into useful products, such as fuels. Since it can be electro-catalytically performed in ambient conditions, it is yet to be proved that assisted by alternative energy resources, such as solar power, it could create new paths towards a more environmentally respectful economy.

Under this perspective, the recently invented crystalline and porous materials Metal-Organic Frameworks could be of great assistance. Their unique properties make them excellent candidates for many applications, one of which is catalysis.

As a result, the ultimate goal of this thesis is to prove that the electrocatalytic behavior of Metal-Organic-Frameworks is suitable for the electroreduction of carbon dioxide to useful products. Various synthesis techniques of these materials are investigated, especially the sonochemical route, which can lead to the formation of these materials under less energy and time compared to the traditional ones.

Keywords:

MOF, Metal organic Frameworks, Synthesis, Sonochemistry, CO2, CO2RR

Περίληψη

Στόχος της παρούσας μεταπτυχιακής εργασίας είναι η σύνθεση νέων υλικών, τα οποία μπορούν να λειτουργήσουν ως καταλύτες για την μετατροπή του διοξειδίου το άνθρακα σε χρήσιμα προϊόντα, όπως καύσιμα. Σε αυτό το πλαίσιο, γίνεται μια προσπάθεια σύνθεσής τους με εναλλακτικούς τρόπους, όπως με τη χρήση της ηχοχημικής μεθόδου, η οποία απαιτεί λιγότερο χρόνο και ενέργεια. Τα υλικά αυτά ονομάζονται Metal Organic Frameworks, MOFs, και διαθέτουν εξαιρετικές ιδιότητες, όπως μεγάλη ειδική επιφάνεια, κρυσταλλικότητα και πορώδες.

Contents

List of Figures

List of Tables

THEORETICAL

1. METAL-ORGANIC FRAMEWORKS

1.1 Introduction

According to Omar M. Yaghi reticular chemistry is defined as linking molecular building blocks by strong bonds to make crystalline extended structures. That is the kind of chemistry lying behind Metal Organic Frameworks (MOFs), invented in 1995 by Omar's research group. By linking metal ions through strong bonds using charged organic linkers (ex. Carboxylates) reticular chemistry has expanded the viewpoints of organic and inorganic chemistry. Thus, this chapter begins with the origins of MOFs and a recommended terminology according to IUPAC, continues with synthesis methods, and concludes with their applications.

1.2 Brief History

Metal Organic frameworks serve as a junction between inorganic and organic chemistry. By being hybrid materials with metal nodes and organic linkers they form a crystalline network with 1D, 2D, or 3D extended periodic structure. Nowadays, there is a great scientific interest in them due to their unique properties, such as high porosity, extremely high surface area, and structural diversity. Consequently, these materials exhibit high potential in many applications, such as gas storage, separation, chemical sensing, and heterogeneous catalysis.[1–6]

From an inorganic point of view, MOF's origins rest at the beginning of the 18th century with the accidental invention of Prussian Blue. According to a book by Stahl[7] in 1706 Johann k. Dippel was preparing "animal oil" in his laboratories from animal materials. Removing the impurities required distillation from potash (K_2CO_3) during which decomposed organic components formed cyanide. Iron from animal blood reacts with cyanide, forming $Na_2Fe(CN)_6$ or $K_2Fe(CN)_6$, components that remain as impurities in the potash. Colormaker J.J. Diesbach working in Dippel's laboratory used the potash that had been used for the 'animal oil' production to create cochineal red, but instead, he created the first coordination polymer, Prussian Blue.[8] This was not proven until 1977, when Buser [8,9] performed an XRD analysis, therefore determining that it consists of a 3D network of Fe(II)/Fe(III) ions bridged by cyanide ligands with the chemical formula of $Fe_4^{3+}(Fe^{2+}(CN)_6)_3 \times H_2O$.

It is worth mentioning that in 1897 Hoffman[10] created a clathrate material (clathrate means basket in Roman), which at that time was considered a molecular solid. History repeating itself, it was the year 1952 when the scientific group of Powel and Rayner were studying Hofmann's complex concluding that its molecular formula was $Ni(CN)_2NH_3C_6H_6$ and by conducting an XRD analysis they found that it was a 2D coordination network of $Ni(CN)_2NH_3$

sheets forming cavities containing benzene moieties as guest molecules. These guest molecules play an important role in the formation of clathrate material due to the structural collapse of the clathrate upon their removal. Powell is until today considered the father of clathrate chemistry. [11]

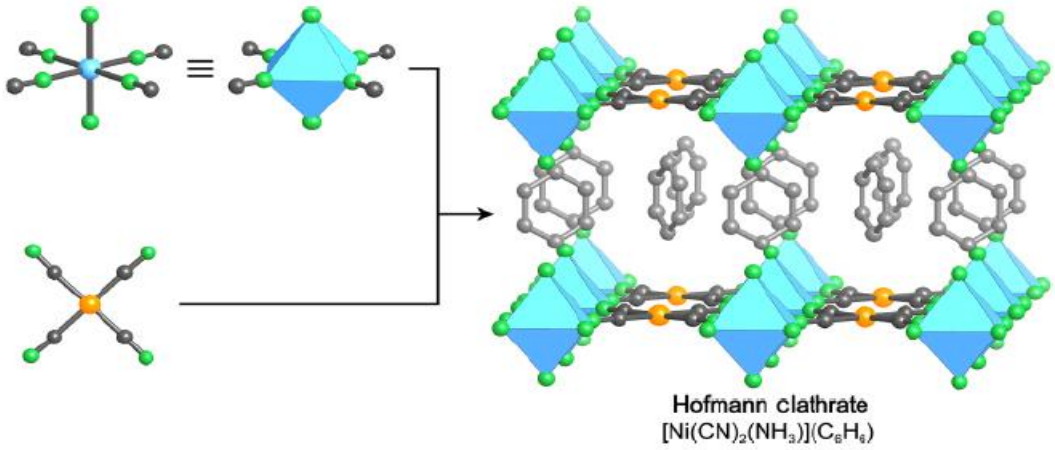

Figure 1: The crystal structure of the original Hofmann clathrate as determined by Herbert M. Powell and coworkers in 1952. Octahedral and square planar nickel moieties are linked by CN− ions into stacked layers of composition $Ni(CN)_2(NH_3)$ that are separated by benzene guests.
Color code: Ni, blue and orange spheres; C, gray; N, green; benzene guest, light gray[12]

The following years after Powell's study, many research groups have been synthesizing clathrate materials.[13,14] It is interesting to note that Iwamoto's scientific group discovered that Hofmann type clathrate materials are defined by the general formula $[M1(NH_3)_2M2(CN)_4]\cdot G$ (G = guest molecule)[15] and M1 and M2 are different divalent metals such Cd or Ni. Alexander F. Wells in the 1950s established the geometric principles of structural inorganic chemistry simplifying the coordination network to nodes and links from a topological point of view.[16]

In the late 1980's the research group of Hoskins and Robson recognized that the topological terms of nodes and connections Wells had proposed, could be applied to the synthesis of coordination networks with predicted architecture. They also realized that these scaffold-like materials have a potential variety of properties.[17] In 1989, they synthesized a 3D coordination network by linking tetrahedral Cu (I) single metal nodes and 4,4',4",4"'-tetracyano-tetra phenylmethane (TCTPM) as an organic linker.[18] During the 1990s, scientific groups were experimenting with different linkers and metals further expanding the idea of controllable synthesis. The Fujita group in Japan, firstly prepared macrocyclic metal complexes in which metals are bridged by linear bidentate(chelate) ligands[19] by using ethylenediamine-capped

Pd^{2+} units bridged by 4,4'-bipyridine. In 1994, the same group reported the formation of a two-dimensional square network material {[Cd(4,4'-bpy)~]$(NO_3)_2$)~ which was studied for its catalytic behavior in cyanosilylation of aldehydes and its XRD analysis confirmed its structure.[20]

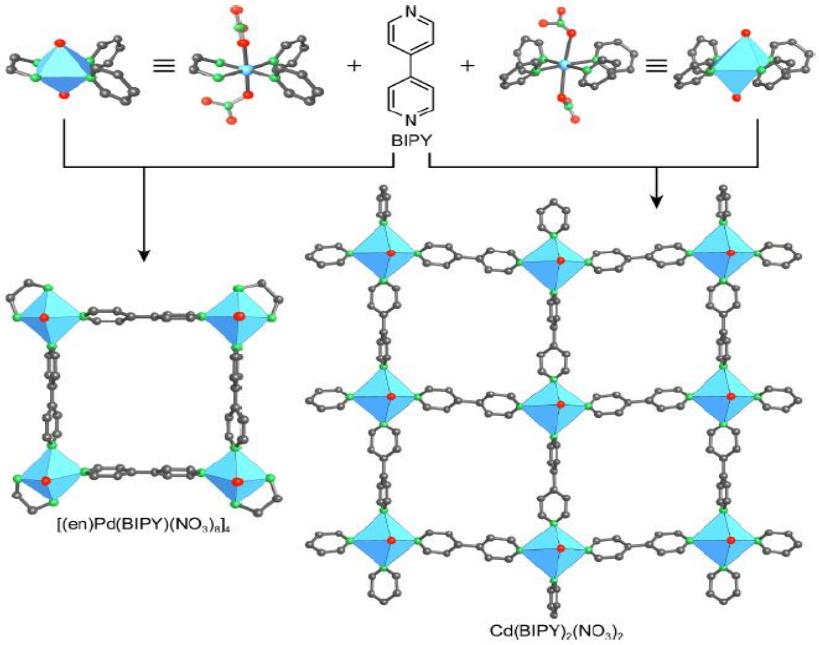

Figure 2: Molecular square synthesized by reacting a capped Pd2+ complex with BIPY. Using Cd^{2+} ions results in the formation of an extended square grid structure of formula Cd $(BIPY)_2(NO_3)_2$. Color code: Pd and Cd, blue; C, gray; N, green; O, red.[12]

The term Metal-Organic Framework was first used by Omar Yaghi and his team. They basically synthesized two $M(BDPY)_2$-related extended coordination networks which set the foundations for the evolution of MOF materials.[12] In October 1995 they published a paper where they synthesized solvothermally a 3D MOF with the molecular formula Cu(4,4'-bpy)$_{1.5}$·$NO_3(H_2O)_{1.25}$.[21] In December of the same year, Yaghi's research group synthesized a 2D coordination network, $CoBTC(Py)_2$, with the molecular formula $[CoC_6H_3(COOH_{0.33})(NC_5H_5)_2{\cdot}0.66NC_5H_5]_\infty$, consisting of alternating layers of pyridine and CoBTC. This network could selectively bind aromatic guests and its crystal lattice could remain thermally stable up to 350 ^oC.[22] Four years later, in 1999, a research team led again by Yaghi, published a study on the synthesis of a MOF based on ZnO_4 tetrahedra and 1,4-benzene dicarboxylate (BDC) building blocks with the molecular formula $[Zn_4O(BDC)_3{\cdot}(DMF)_8(C_6H_5Cl)]_\infty$ that is stable up to 300 ˚C, known as MOF–5. [23]

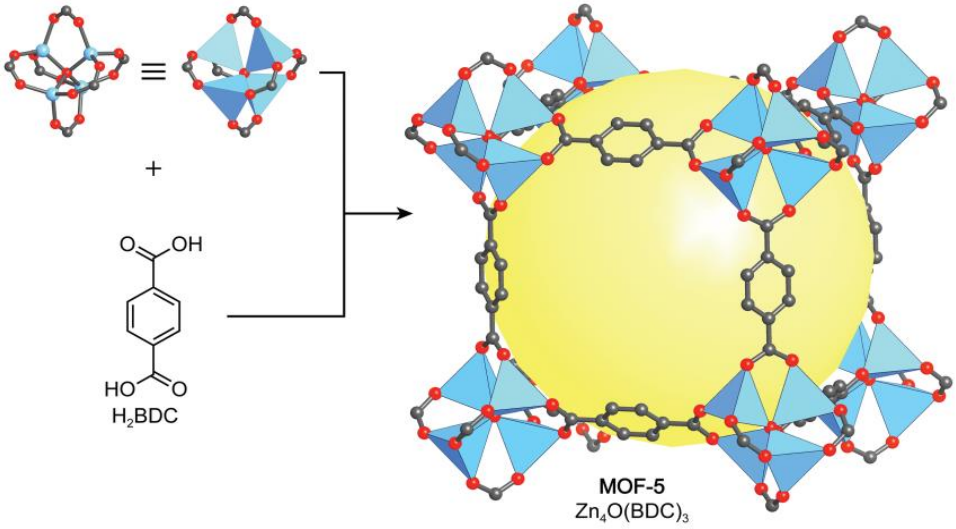

Figure 3: MOF – 5. Top left the ZnO_4 tetrahedra – Bottom left the linker BDC. Right: Single-crystal X-Ray structure of MOF-5. Each of the eight corners is occupied by a tetrahedral $[OZn_4(CO_2)_6]$ cluster. The yellow sphere represents the cavity of the framework. Color code: Zn, blue polyhedron; O, red; C, grey;[24]

In the past two decades, more than 20.000 MOFs have been synthesized due to the flexibility in pore size, functionality, and architecture presented by these materials. [25] As observed from diagram 1 scientific interest and research is increasing rapidly since the invention of MOF-5.

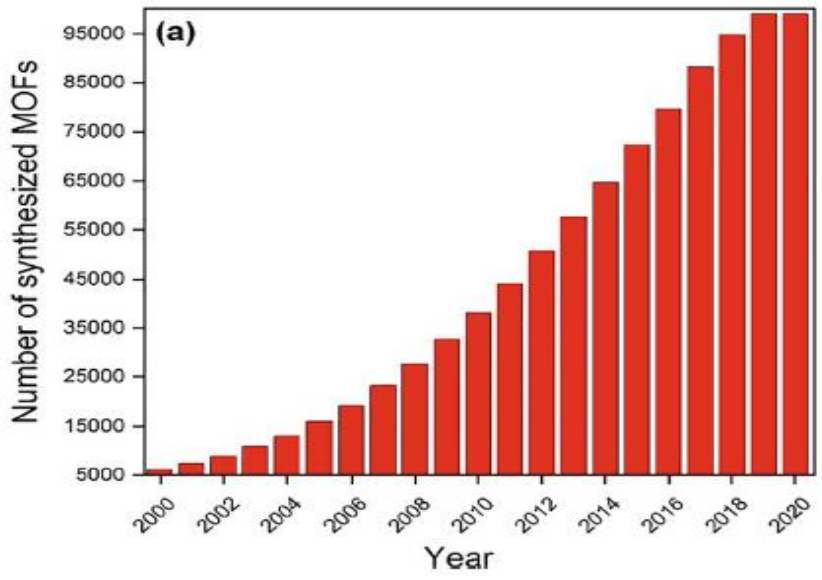

Figure 4: Number of MOFs reported in the Cambridge Structural Database (CSD) according to years. Retrieved from the CSD on 4th March 2020. [26]

1.3 Terminology

Due to MOF's innovative character providing a rapidly growing expansion of their field of study by multiple research groups, appropriate terminology must be established. Another reason for this urgency is the interdisciplinary nature of MOFs, which lays its roots in both coordination and inorganic chemistry causing occasional misunderstandings among the scientific community. To avoid these misconceptions and after years of research, the International Union of Pure and Applied Chemistry (IUPAC) set the required guidelines in 2013, according to which terminology is well established. [27]

A *coordination compound* is any compound that contains a coordination entity. A coordination entity is an ion or neutral molecule that is composed of a central atom, usually, that of a metal, to which is attached to a surrounding array of atoms or groups of atoms, each of which is called ligands.

A *coordination polymer* is a coordination compound with repeating coordination entities extending in 1, 2, or 3 dimensions.

A *coordination network* is a coordination compound extending, through repeating coordination entities, in 1 dimension, but with cross-links between two or more individual chains, loops, or spiro-links, or a coordination compound extending through repeating coordination entities in 2 or 3 dimensions.

A *metal-organic framework*, abbreviated to MOF, is a coordination network with organic ligands containing potential voids.

It shall be noted that there is no commonly accepted assigning of names for MOFs. MOFs' nomenclature can be either their chemical formula or type (ZIF-68, MOF-74, etc.) or even the associated university/facility (UiO, MIL) accompanied by a number. [28]

1.4 Synthesis

Conventional

According to the literature, conventional synthesis is categorized as solvothermal and non-solvothermal, based on the temperature range the synthesis reaction is occurring. [29,30] Generally, non-solvothermal synthesis is carried out at room temperatures and ambient pressure in open flasks below the solvent's boiling point. On the other hand, Rabenau [31] defies the solvothermal synthesis route as being carried out at or above the solvent's boiling point in closed vessels at elevated pressure caused by solvent vapor or produced by a pump. The

term solvothermal is generally implying any solvent, whereas the term hydrothermal refers to water as a solvent.

As far as the non-solvothermal method is concerned, the parameters that must be carefully studied for the formation of the precipitation are the reagent concentrations, the pH, and the temperature. Increasing the temperature while using evaporating solvent results in higher yields by achieving the required nucleation conditions.[32]

The solvothermal route has been, and still is, the most common way of synthesizing MOFs in laboratories since their discovery by O.Yaghi in 1995. Typically, the procedure involves the mixing of the reagents, the organic linker and the metal salt, in the solvent and the placement of the final solution in sealed reactors (most commonly known as autoclaves) at high temperatures for hours or even days. This route leads to better crystallinity and higher yield than the non-solvothermal. [33]

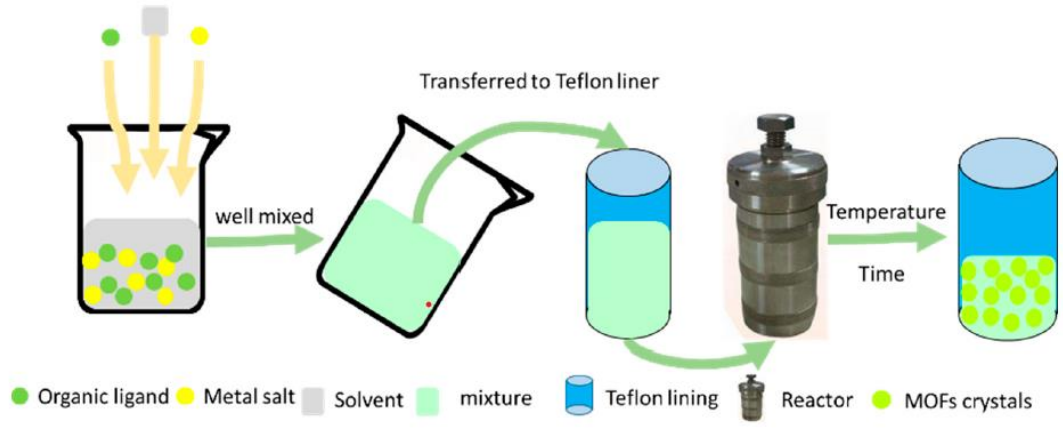

Figure 4: Schematic presentation of solvothermal synthesis [34]

As mentioned before, solvothermal/hydrothermal route of synthesis may take up to several days due to conventional heating. Thus, there have been developed alternative techniques to facilitate MOFs production by decreasing reaction time and as a result, demanding less energy.

Microwave-Assisted

Microwave heating was discovered accidentally in 1940's by P.L. Spencer at the Raytheon Corporation when a candy bar melted in his pocket while he was working on radar related research project, a new type of magnetron. Intrigued by this fact, he went even further by placing other foods near the magnetron and watched them change their physical status due

to increasing temperature after some period.[35] This observation led to the invention of the microwave oven, which revolutionized food industry.

Microwaves are electromagnetic waves with wavelengths in the 1 m to 1 mm range (300 MHz to 300 GHz) and the frequency of radiation used in domestic microwave ovens is 2.45 GHz (12.24 cm). Microwave irradiation offers controllable heat transfer which can not only be used for food heating but can also be employed for a variety of chemical applications, such as material synthesis.

The method is based on the interaction of electromagnetic waves with any material containing mobile electric charges, such as polar molecules in a solvent or conducting ions in a solid. Contrary to classical solvothermal methods, where thermal energy is transferred from the heat source to the solution through the reaction vessel, in MW synthesis the irradiation interacts directly with the reactants, resulting in more efficient and faster heating. Additionally, in MW synthesis crystallization occurs at the hot spots that form due to the direct heating of the solvent, in contrast to the wall of the reactor vessel as with conventional heating methods. Consequently, it is much faster and results in a smaller particle size.[36] Research in this field has proven that MOFs can be synthesized via a microwave-assisted process, firstly published in 2006 by a team at the University of Chicago Illinois.[37]

Practically, in microwave synthesis, a substrate mixture in a suitable solvent is transferred to a Teflon vessel, sealed, and placed in the microwave unit, and heated for the appropriate time at the set temperature. The microwave approach, where an applied oscillating electric field is coupled with the permanent dipole moment of the molecules in the synthesis medium inducing molecular rotations, results in rapid heating of the liquid phase.[38]

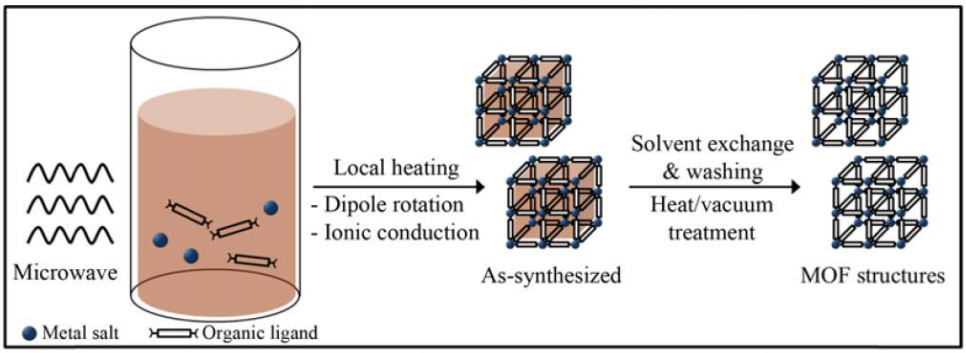

Figure 5: Schematic presentation of microwave assisted synthesis method [39]

Electrochemical

The electrochemical synthesis of MOFs was first reported in 2005 by researchers at BASF.[40] Their main objective was the exclusion of anions, such as nitrate, perchlorate, or chloride, during the syntheses, which are of concern to large-scale production processes.

The synthesis consisted of immersing a copper plate in a solution containing the organic linker, 1,3,5- benzene tricarboxylic acid (BTC), and an electrolyte. The copper electrode, was used as the source of Cu(II) ions. When a certain current or voltage was applied, the Cu(II) ions were released from the copper electrode to the solution and reacted with the dissolved linker. This technique resulted in the fabrication of a powder of HKUST-1. [41]

Currently, the electrosynthesis of MOFs can be classified in two main methods: (i) the before mentioned anodic dissolution and (ii) the cathodic deposition. [36]

In the anodic deposition, as shown in Figure 6, an applied electric potential induces the release of metal ions from the electrode, which then react with an organic linker present in the solution leading to the formation of a MOF film. In this case, the use of a metallic electrode (instead of metal salts) as the source of metal cations avoids the formation of any corrosive anions (mainly, nitrate and acetate anions) or any by-products. The anodic dissolution is typically carried out in a two-electrode set-up without a reference electrode, and the use of protic solvents is usually needed to ensure the evolution of hydrogen and avoid the reduction of metal ions at the counter electrode. In addition, the use of a sacrificial compound (e.g., acrylonitrile, acrylic or maleic esters) that are preferentially reduced or a counter electrode with a suitable overpotential for hydrogen evolution is recommended.[36,42]

In the cathodic deposition, a solution containing the organic linker, the metal ions, and a so-called pro-base is contacted with a cathodic surface (Figure 7). In this approach, the MOF film deposition results from increasing the pH near the cathodic surface, where the electrochemical reduction of the pro-base occurs. An example of a pro-base is the nitrite ions coming from the reduction of nitrates, which can deprotonate the organic linker and form the MOF.[36,43]

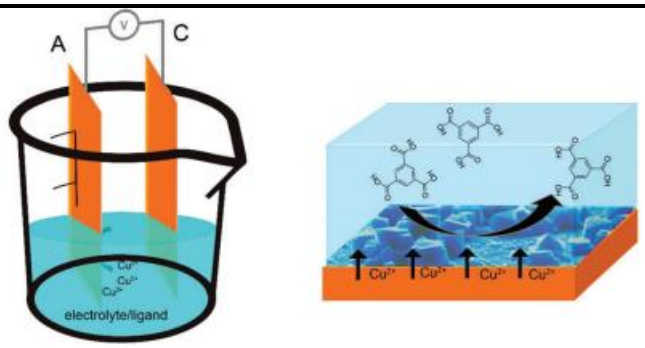

Figure 6: Electrosynthesis of MOFs by anodic dissolution[36]

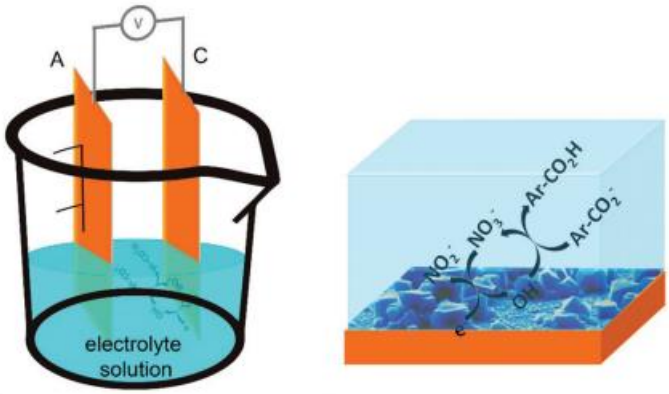

Figure 7: electrosynthesis of MOFs by cathodic deposition[36]

In a comparative study on the influence of the synthesis procedure on the properties of HKUST-1, the compound was synthesized using solvothermal, ambient pressure, and electrochemical routes in pure ethanol and ethanol/water mixtures.[44] Although XRD investigations demonstrated that in all cases HKUST-1 was formed, TG experiments, elemental analyses, and sorption experiments showed the inferior quality of the electrochemically synthesized product. This was explained by the incorporation of linker molecules and/or the conducting salt in the pores during crystallization.[32]

Mechanochemical

Mechanochemical synthesis is a well-known technique in metallurgy and mineral processing but within the last few decades it has expanded rapidly into many areas of chemistry such as catalysis, inorganic chemistry and pharmaceutical synthesis.[45–47] The central concept behind this synthesis method is to promote chemical reactions by milling or grinding solids without any or with only minimal amounts of solvents.[48,49] Typically, the studies of mechanochemical mechanism between solids are introduced through mechanical energy such as ball milling.
In general, the mechanical milling process is higher in energy and ensures the reproducibility between batches. In addition to the solvent-free conditions, this approach leads to a faster and more efficient synthesis of MOFs obtaining quantitative yields and allows to use MOF precursors with low solubility such as oxides, hydroxides, and carbonates. However, it should be noted that despite the solvent-free synthesis, purification may still be needed and may require a solvent.[50] Nevertheless this synthetic approach is the most environmentally friendly process to produce MOFs and could reduce significantly the production cost.[51]

The three different mechanochemical approaches used for MOF production are i)Solvent-Free Grinding (SFG), which is the simplest method and avoids the use of solvent; ii)Liquid-Assisted Grinding (LAG), which is more versatile, and quicker, as it uses catalytic amounts of liquid phases, which increase the mobility of the reagents; and finally, iii)Ion-and-Liquid Assisted Grinding (ILAG), which uses a catalytic liquid with traces of salt additives to accelerate the MOF formation. Using these techniques, the synthesis for almost all families of MOFs has been demonstrated, and selected studies will be explained in this section.[36]

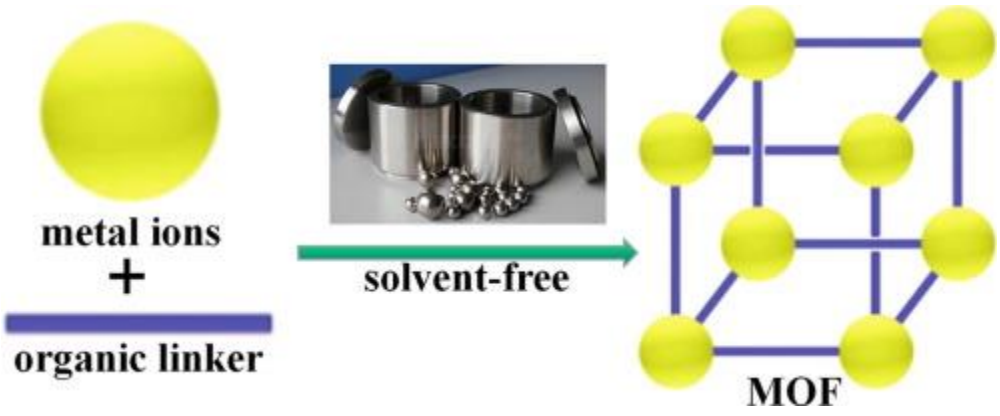

Figure 8: Mechanochemical MOF synthesis. Typically conducted via ball milling[52]

Sonochemical

General

Ultrasound is defined as a sound wave with a frequency exceeding 16 kHz and with a standard upper limit of 5 MHz for gases, or 500 MHz for liquids and solids. The application of ultrasound in the physical and biological sciences can be divided into two main groups: (i) low frequency or high-power ultrasound (20-100 kHz) and (ii) high frequency or diagnostic ultrasound (2-10 MHz).[53] The use of ultrasound has found many applications in the chemical and manufacturing industries where it is used to improve synthetic and catalytic processes and to create new products.[54]

Sound as a wave propagates in a medium as a change in pressure causing compression and dilution regions and creating vibrations in the molecules of the medium. More specifically, in liquids and gases it is transmitted in the direction of the wave causing longitudinal waves and in solids causing transverse vibrations perpendicular to the wave propagation.

Sonication of a liquid medium generates chemical and physical effects.[55–58]It is characterized by unique short times, high energy and pressure, as seen in Figure 9.[59] The chemical effects of ultrasound do not come directly from the interaction of the acoustic waves with the molecules, instead, the effects come from acoustic cavitation process. Cavitation refers to creating a cavity in a liquid medium. However, the cavitation process involves the formation, growth, and the collapse of a microbubble in an ultrasonically irradiated solution.[54]

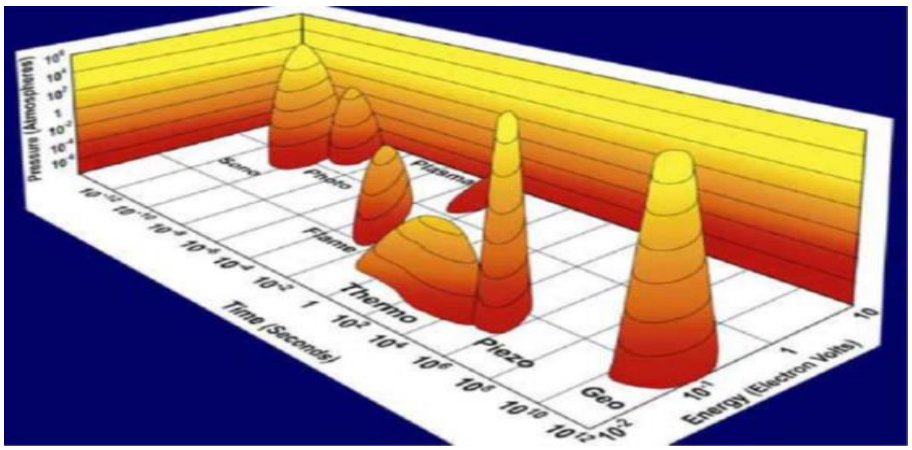

Figure 9: Islands of chemistry as a function of time, pressure, and energy. Sonochemistry occupies a unique short-time, high-energy, and high-pressure space [59]

The medium through which ultrasound travels through experiences alternating acoustic pressure cycles. During rarefaction, the negative pressure causes a pulling effect causing bubble nucleation. In this case, the cohesive force between solvent molecules needs to be

overcome to create a bubble/cavity. For cavitation bubble to form, a high negative pressure is required. Theoretical negative pressure required to form a cavity in water is of the order of a few hundred atmospheres[60]. However, experiments have shown that the actual pressure required is much less than the theoretical value. This is because of the advantage of having impurities, dissolved gases and particulates in water. Once a bubble/cavity is formed, it undergoes oscillations under the pressure variation.

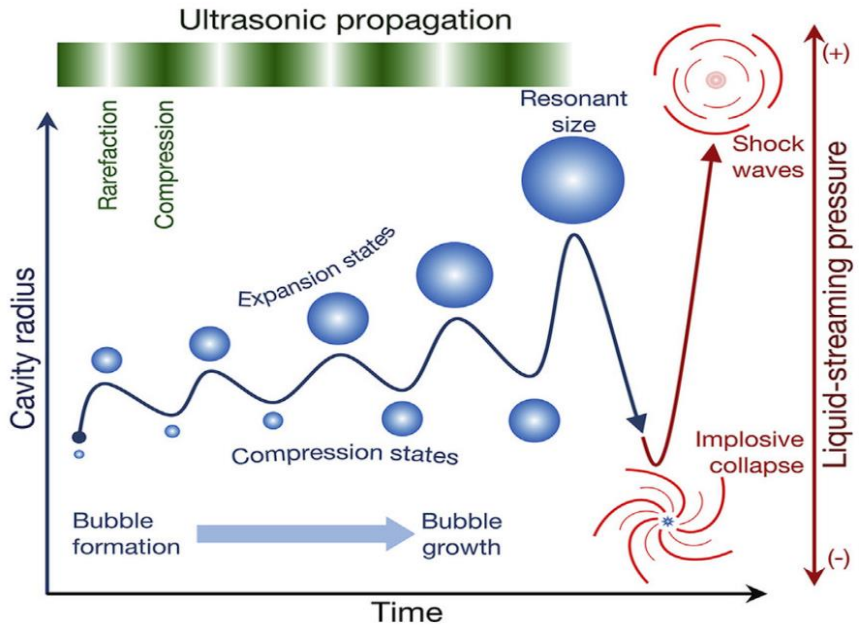

Figure 10: Formation and collapse of bubbles formed in the solution after sonication, termed acoustic cavitation, produces very high local temperatures (~5,000 K) and pressures (~1,000 bar), and results in extremely fast heating and cooling rates (>1010 K/s) producing fine crystallites[59]

The effect of ultrasound on the liquid and colloid systems is mainly due to cavitation. This is the occurrence of vapor formation and the release of air which is caused by a decrease in pressure in the liquid because high-intensity acoustic wave spreads through it. Though, in fact, the fall in pressure leads to the release of air dissolved from the liquid and the formation of gas voids, cavities. The pressure in the cavities is more than the pressure of saturated vapor, therefore, the cavity starts to form from a nucleus, increases to a finite shape and then collapses. The entire method only takes a few milliseconds. For cavity formation, the nuclei are microscopic bubbles. They form small cracks in the container surface and suspended particles on the edges of the vessels. When the bubbles fall, a faint glow is observed due to the heating of the gas in high pressure-induced bubbles. Thus, the bubble fall leads to a significant increase in temperature and the high-pressure difference in the surrounding liquid of the bubble[61,62, 33]

The use of ultrasonic waves and cavitation has many important effects as it applies to chemical processes. The resonant bubbles act as the instigator, increasing the area of contact among the reagents. In addition, thermal effects and pressure are due to the disruption of differential particle aggregates, which also increase the contact area.

Sonochemical Synthesis of MOFs

The sonochemical method was first used for the synthesis of a MOF, namely $Zn_3(BTC)_2$, in 2008 where zinc acetate and H_3BTC were mixed in 20% ethanol and subjected to sonication for 90 minutes. However, high yield (75.3%) of the product was achieved even after 5-minute sonication. [63]

In the same year, another research group by using sonication was able to decrease the time of synthesis of MOF-5 from 24 h (conventional heating) to 75 min. Solutions of zinc nitrate and terephthalic acid in 1-methyl-2-pyrrolidone were mixed in nitrogen atmosphere. Then, the mixture was transferred into a reactor and subjected to sonication for 10 ± 75 min. Precipitation of MOF-5 commences even after 8 min of sonication.[64]

In addition, HKUST-1 was synthesized via this method from an aqueous solution of copper acetate and a solution of H_3BTC in a mixture of DMF with ethanol. The starting compounds were placed into a container mounted in a water bath and were subjected to sonication at a frequency of 40 kHz for some time (from 5 to 60 min). The yield of the product was from 62.6% to 85.1% depending on the synthesis duration.[65]

The Schlesinger group made a study comparing six different methods of synthesis of HKUST-1: synthesis at atmospheric pressure with heating under reflux, solvothermal synthesis, electrochemical synthesis, microwaving, mechanochemical synthesis (with addition of a solvent) and sonication. All procedures gave the pure phase of the product. Maximal yield at minimal synthesis duration was achieved by means of microwave radiation.[66]

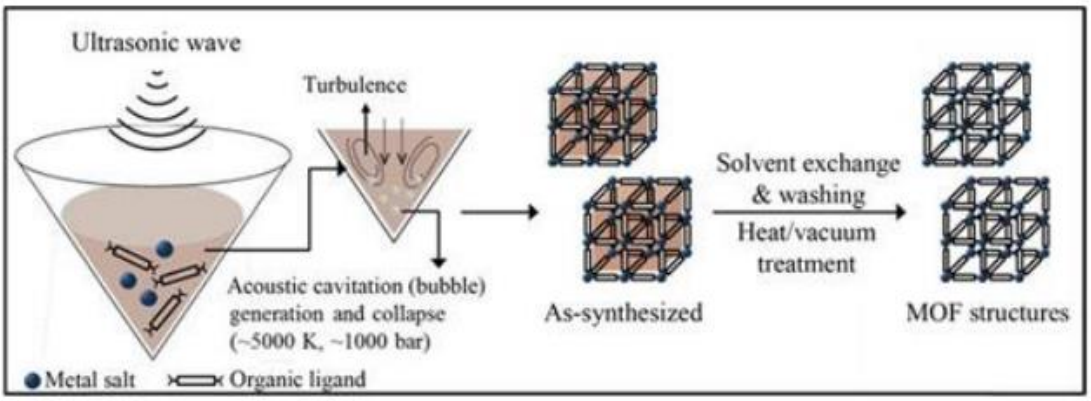

Figure 11: Sonochemical Synthesis of MOF structures[39]

1.5 Applications

Gas Storage

The application of MOFs on gas storage is critical since they are porous materials. For CO_2 collection from flue gas, several MOFs have been synthesized.[67] Traditional gas absorption methods' greatest flaws are their excessively large equipment sizes and significant energy consumption. MOFs, on the other hand, have a cheap cost and are reasonably easy to renew, among other advantages. Furthermore, most show potential as hydrogen, methane, and other sustainable energy storage materials. MOFs have previously attracted a lot of interest and have shown promising outcomes.

Biomedical/Drug Deliver

Because they offer important qualities including high BET surface area, great biocompatibility, and functional diversity, certain MOF materials have a significant quantity of drug loading ability. On a nanoscale scale, some of them might be used to develop new theragnostic nanomedical devices. Some MOFs on the mesoporous scale may also have the capacity to load biological molecules into their pores, such as anticancer drugs. Patricia et al. demonstrated for the first time the extraordinary potential of MIL-100 and MIL-101 to host and distribute Ibuprofen. They also mentioned the vast potential for developing novel MOFs, such as their ability to adapt to the structure of medications and their dose needs.

Asymmetric Catalysis

Because of their pore structures and large specific surface area, MOFs can be functionalized using metal ions and ligands to produce catalytic sites. In the last few decades, researchers have recognized that MOFs could be used in asymmetric catalysts after incorporation of a chiral ligand or proper chiral catalytic units or open metal sites or inside pores.[68] POST-1 is the first example of MOFs which exhibited catalytic features for an asymmetric chemical reaction

as reported by Kim et al. MOFs as asymmetric catalysts have the benefit of avoiding the time-consuming separation procedure necessary in a general synthesis technique that results in racemic mixtures, as well as not requiring huge amounts of chiral agents as in the classic stoichiometric synthetic method.

Adsorptive Separations

The gas separation process being realized by MOF materials is derived from the differences in adsorption/desorption behavior of components of a mixture.[69] Rational design about the pore sizes and other properties at the molecular level may result in unique interactions with certain guest molecules rather than others and thus achieve unusual chemical-physical adsorption.

2. CO_2 REDUCTION

2.1 The Environmental Aspect

One of the greatest challenges facing humanity in the 21st century is finding a reliable, safe, and carbon-neutral energy source. The world population is projected to reach 12 billion by the year 2100 (compared to 7.7 billion today).[70] At the same time, living standards continue to rise in the developing world, resulting in increasing global energy consumption.

Today, global energy production is mainly based on the burning of fossil fuels, as shown in Figure 12. From energy sources, coal, oil and natural gas account for 80.9% of current global energy supply. The rest is provided by nuclear energy, hydroelectric power, while renewable energy sources represent only 2.2%. Figure 13 shows an estimate of global energy consumption by 2050. It is estimated that coal and natural gas will present a slight increasing trend and nuclear power will remail stable. On the other hand, the use of renewable energy resources will increase rapidly over the next 30 years. [71]

Fossil fuel reserves are not inexhaustible. At current consumption rates, the known and economically viable reserves of oil, gas and coal are sufficient for about 30, 40 and 70 years, respectively,[72] as the projections illustrate in Figure 13. Moreover, as far as oil is concerned, it is the raw material for several chemical products that are essential in everyday life and its depletion will lead to the deprivation of these products. Given both the growing world population and the growing trend of global energy needs, alternatives and more permanent solutions will soon have to be found.

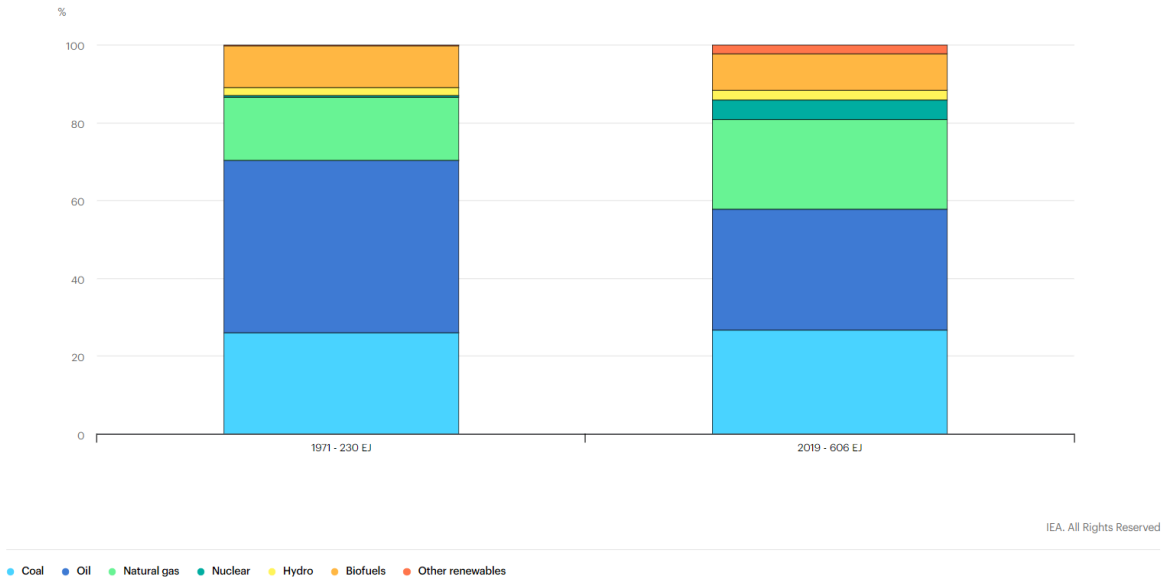

Figure 12: Total energy supply 1971 vs. 2019 - Data provided by IEA[73]

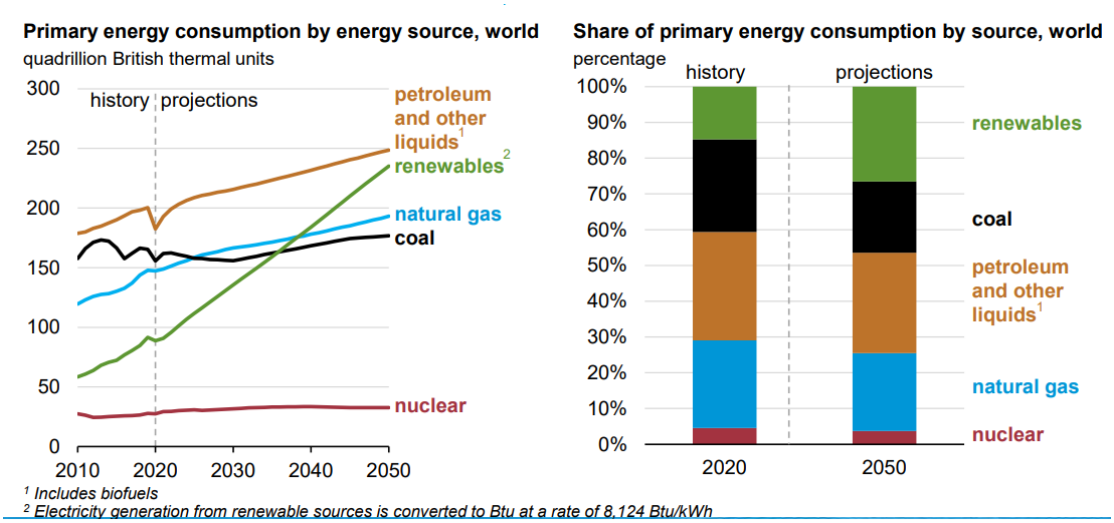

Figure 13: Global primary energy consumption by energy source(left) and global share of primary energy consumption(right) in 2020 and projection for 2050[74]

CO_2 and Climate Change

Carbon dioxide (CO_2) is the primary greenhouse gas emitted through human activities. In 2020, CO_2 accounted for about 79% of all U.S. greenhouse gas emissions from human activities. Carbon dioxide is naturally present in the atmosphere as part of the Earth's carbon cycle (the natural circulation of carbon among the atmosphere, oceans, soil, plants, and animals). Human activities are altering the carbon cycle–both by adding more CO_2 to the atmosphere and by influencing the ability of natural sinks, like forests and soils, to remove and store CO_2 from the atmosphere. While CO_2 emissions come from a variety of natural sources, human-related emissions are responsible for the increase that has occurred in the atmosphere since the industrial revolution.[75]

The excessive combustion of fossil fuels has caused massive carbon dioxide (CO_2) emissions, leading to rapid global environmental changes such as global warming, air pollution, desertification, acid rains, rise in sea levels, and extreme weather conditions.[76] The threats to human life and the environment due to high CO_2 emissions are increasing day by day with growing energy demands.

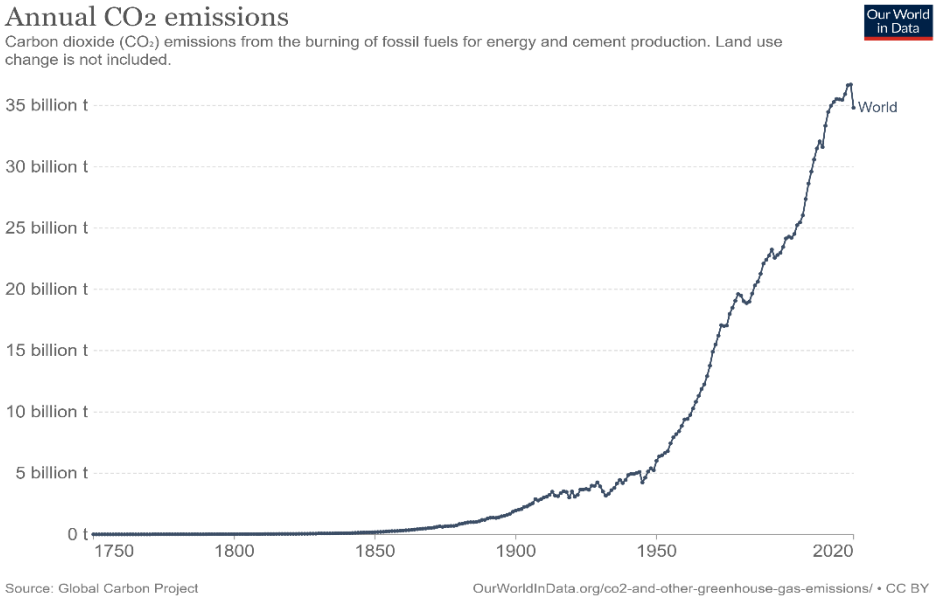

Figure 14: CO_2 emissions from the burning of fossil fuels and cement production (land use not included) [77]

According to the Global Warming Potential (GWP) updates by the United States Environmental Protection Agency (EPA), CO_2 has a GWP value of 1, which is lower than the value of CH_4, N_2O, chlorofluorocarbons (CFCs), hydrofluorocarbons (HFCs), and other greenhouse gases. However, the CO_2 absorption energy is much higher as it has remained for thousands of years in the atmosphere compared to other greenhouse gases, as shown in Figure 15, reflecting the severe contribution of CO_2 to global warming. [78]

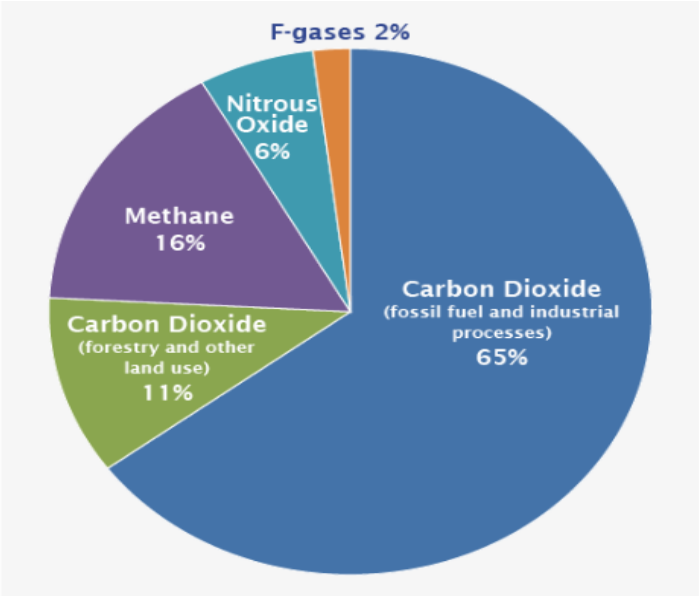

Figure 15: Global Greenhouse Gas emission by gas – IPCC [79]

The concentration of CO_2 in the atmosphere is constantly increasing over time. In Figure 16 shows an increase in atmospheric carbon dioxide over the last 60 years. The data comes from the Mauna Loa Observatory of the US National Oceanic and Atmospheric Administration (NOAA) in Hawaii. The rate of increase of CO_2 concentrations is constantly increasing and since 2000, the global atmospheric carbon dioxide amount has grown by 12 percent.[80]

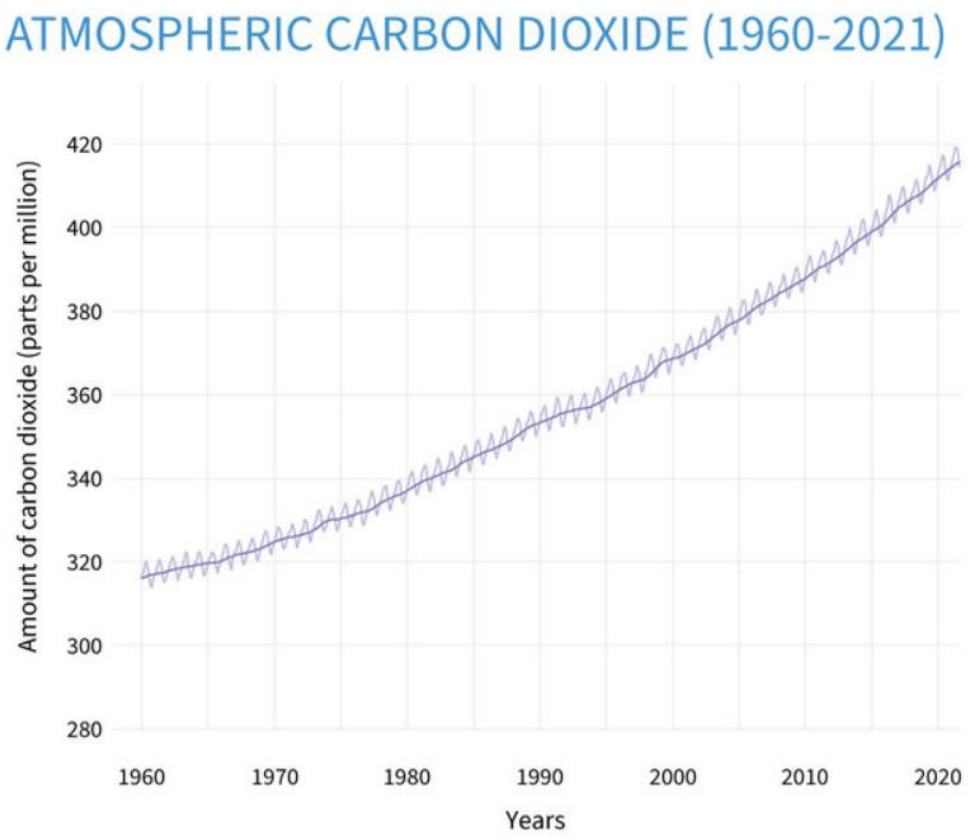

Figure 16: Average carbon dioxide measurements since 1960 in parts per million (ppm). The long-term trend of rising carbon dioxide levels is driven by human activities. NOAA Climate.gov image, based on data from NOAA Global Monitoring Lab.[81]

The Intergovernmental Panel on Climate Change (IPCC) was established by the UN and the World Meteorological Organization in 1988.[82] The committee presented a report in 1990 reflecting the views of 400 scientists on anthropogenic climate change. According to this report, the problem of rising temperature was real and had to be addressed immediately. The Intergovernmental Commission's findings prompted governments to establish the United Nations Framework Convention on Climate Change (UNFCCC). In 1992 at the Rio de Janeiro Summit (also known as the Earth Conservation Summit), 167 states signed a non-binding Framework Convention on Climate Change.[83]

It followed the Kyoto Protocol in 1997 in which 38 industrialized countries pledged to reduce greenhouse gas emissions by 5.2% by 2010.[84] In December 2015, the 21st session of the Conference of the Parties (COP 21) of the United Nations Framework Convention on Climate Change (UNFCCC) and the 11th session of the Conference of the Parties to the Kyoto Protocol (CMP 11) took place in Paris. The new global agreement on climate change in Paris provides for an action plan to reduce global warming to below 2 °C. The main element of the Paris Agreement is to maintain the increase of the average global temperature below 2 °C in relation to the pre-industrial levels and to continue the efforts to limit it to 1.5 °C.[85]

Ways of Reducing CO_2 emissions

CO_2 can potentially be used to produce synthetic fuels such as methanol and biofuels or as raw material to produce chemicals like polymers, organic acids and alcohols or even to produce a wide range of other products. To date, CO_2 has been used successfully in the production of refrigerants, beverages, fire extinguishers, water treatment processes, in the food industry and many other smaller scale applications.

The main strategies to reduce CO_2 emissions deal with the circular carbon economy (CCE), a holistic approach that consists of Reduce, Reuse, Recycle and Remove (4Rs) of CO_2. The reuse of CO_2 is categorized to search for low carbon energy alternatives such as wind, solar and hydro energy for replacing fossil fuels. Today, reducing CO_2 emissions, while converting it into useful products appears as a necessary demand for environmental protection. There are different technologies proposed to reduce CO_2 emissions, which are mainly based on the following approaches:[82]

- CO_2 collection and geological isolation and
- CO_2 conversion of into useful products

The second approach regarding CO_2 conversion into useful products seems the most attractive and promising solution. It can be achieved via chemical methods, via photocatalytic or electrocatalytic reduction. However, there are still some significant challenges regarding the practical application of mitigation technologies, which include

- High cost of CO_2 reduction technologies
- Chemical and electrochemical conversion requires high energy
- Restrictions on market size and lack of investment incentives

- Lack of incentives for industrial commitment and production of CO_2-based chemicals
- Insufficient socio-economic information

Despite the challenges, the capture, conversion, and utilization of CO_2 is still recognized as a viable and promising field of research in energy and the environmental sectors. The main methods of reducing CO_2 include the following:

- Radiochemical method. Products such as HCOOH and HCHO can be produced in aqueous solutions with the energy supply derived from γ-radiation.

$$CO_2 \xrightarrow{radiation\ \gamma} HCOOH, HCHO$$

- Chemical reduction from metals (metallurgy field), which takes place at relatively high temperatures.

$$2Mg + CO_2 \rightarrow 2MgO + C$$
$$Sn + 2CO_2 \rightarrow 2SnO_2 + 2CO$$
$$2Na + 2CO_2 \rightarrow Na_2C_2O_4$$

- Thermochemistry

$$CO_2 \xrightarrow{Ce^{4+},\ T>900C} CO + {}^1/_2\, O_2$$

- Photochemistry

$$CO_2 \overset{hv}{\rightarrow} CO, HCOOH, HCHO$$

- Electrochemical

$$CO_2 + xe^- + xH^+ \overset{ev}{\rightarrow} CO, HCOOH, (COO_2) \dots$$

- Biochemical

$$CO_2 + 4H_2 \xrightarrow{bacteria} CH_4 + 2H_2O$$

- Biophotochemistry

$$CO_2 + oxoglutaric\ acid \overset{hv}{\rightarrow} isocitric\ acid$$

- Photoelectrochemistry

$$CO_2 + 2e^- + 2H^+ \xrightarrow{ev,hv,semiconductor} CO + H_2O$$

- Bioelectrochemistry

$$CO_2 + oxoglutaric\ acid \xrightarrow{enzyme,ev,methylviologen} isocitric\ acid$$

- Biophotoelectrochemistry

$$CO_2 \xrightarrow{ev,hv,enzyme,\ methylviologen,p-lhP} HCOOH$$

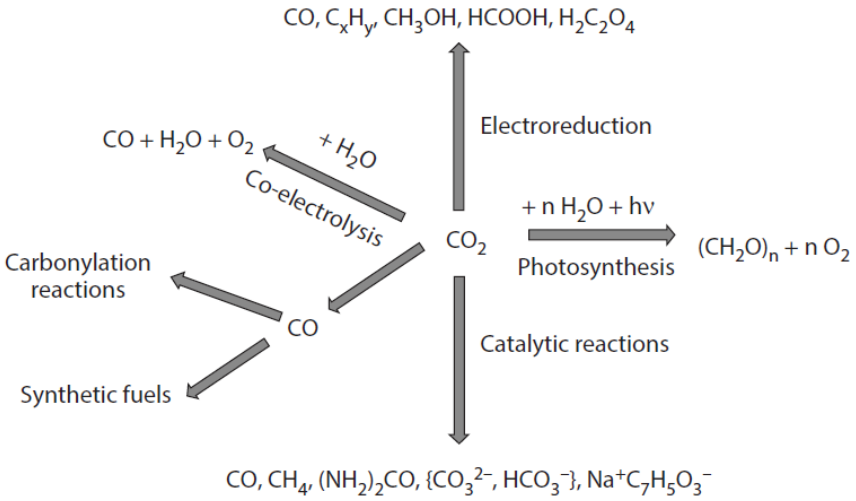

Figure 17: The main methods of converting carbon dioxide into useful products - the chemical compounds that can be obtained from each method[86]

2.2 Electrochemical CO_2 Reduction

Electrocatalytic CO_2 reduction reaction (CO2RR) is a promising strategy due to its easy operating system, simple constructions, operational at neutral pH, ambient temperature and atmospheric pressure, and low energy utilization to produce valuable chemicals and fuels such as formic acid, methane, ethanol, and carbon using renewable electricity. Therefore, CO2RR coupling with renewable energy sources can effectively achieve a carbon-neutral energy cycle and hydrocarbon products with high activity, stability, and selectivity.

Synthetic fuels derived from CO_2 can be a dynamic component of a carbon energy cycle, according to the following equation:[87]

$$CO_2 + energy \rightarrow fuels \rightarrow CO_2 + energy$$

The fuel can be carbon monoxide, methane, longer chain hydrocarbons, methanol or C2-C3 alcohols. Electricity can be generated by various methods. In order to accomplish this goal, one should devise sustainable systems that can produce fuels by converting carbon dioxide and water, utilizing naturally available solar, wind or hydro energy.[88]

The liquid CO_2 electrolysis products are more efficient energy storage media, as shown in Table 1, than thermal and mechanical storage, batteries, and hydrogen. A cost-effective electrochemical reduction of carbon dioxide will allow a shift towards a sustainable energy economy. In combination with a renewable energy source, CO_2 electrospinning could lead to carbon-neutral fuels or industrial chemicals, which are now commonly derived from petroleum.[89]

A necessary condition for such a process to take place is the development of active and selective catalysts, which allow the reduction of CO_2 with high current density and high yields of the desired products without a significant quantity of by-products.

The main factors that determine the efficiency of the energy storage medium are the energy density by weight and volume. In Table 1 a comparison of different forms of energy storage is presented. Mineral energy sources are given as a reference point for comparison with other forms.[90]

Table 1: Comparison of Different Forms of Energy Stores. N/A = Not Applicable.NF: Value not found in literature. SS: Only utilized on small scale

Energy Storage Type	Energy Density		Cycle Efficiency	Capacity (MW)	Capital ($/kW)
	kJ/kg	MJ/m^3			
Fossil Fuels					
Crude Oil	42000	37000	N/A	N/A	N/A
Coal	32000	42000	N/A	N/A	N/A
Gasoline	46400	34200	N/A	N/A	N/A
Diesel	46000	37300	N/A	N/A	N/A
CO_2 Electrolysis					
Products					
Methane	53600	39	0.122	SS	SS
Methanol	21000	17000	0.488	SS	SS
FT Diesel (HHV)	47400		0.368	SS	SS

Syngas (2:1 $CO:H_2$) (HHV)	24700		0.473	SS	SS
Biochemical Pathway					
Ethanol	28000	22000	0.6	N/A	N/A
Biodiesel	38600	34000	0.8	N/A	N/A
Thermal					
Water (100C -> 40C)	250	250	0.4-0.5	NF	NF
Inorganic Salt, heat fusion >300C	>300	>300	0.6-0.7	NF	NF
Mechanical					
Pumped Hydro, 100m head	1	1	0.65-0.8	1000-3000	500-1500
Compressed Air		~15	0.4-0.5	200-500	250-1000
Flywheel, steel	30-120	240-950	0.8-0.95	20-40	100-300
Electrochemical (Battery)					
Lead-Acid	40-140	100-900	0.7-0.8	400-100	NF
Lithium ion	700	1400	0.7-0.9	200	600
Water Electrolysis					
Hydrogen, gas	120000	10	0.4-0.6	100	800
Hydrogen, liquid	120000	8700	NF	NF	NF
Hydrogen, metal hydride	2000-9000	5000-15000	NF	NF	NF

This intense interest of scientists is due to the ever-increasing concentration of CO_2 in the atmosphere, which led to the need to find methods of its capture and, in general, to reduce its emissions into the atmosphere. Although much work has been done in this area, to date there is no industrially viable method of producing a product. A method for industrial exploitation must have the following characteristics:

- To be performed at low values of cathodic potential, close to equilibrium potential, in order to reduce energy requirements.
- To have high% power efficiency (Faradaic Efficiency, % FE).
- To have high conversion speed, that is the high current density.
- To have a high selectivity to a product, which must be easily separated.

Electrochemical reduction of CO_2 was first studied in 1870 by Royer,[91] who reported the reduction of CO_2 to formic acid on Zn electrodes. In the 1990s catalytic efficiency was enhanced by the introduction of gas diffusion electrodes, which increased the catalytic surface, thus the contact area of gas and liquid phases. As mentioned before, the industrial application is not yet feasible due to high cost, low product selectivity, and poor stability.

Moreover, metal CO_2 batteries, which are another type of utilization form of CO_2 electroreduction, can convert chemical energy into electrical energy. Among all CO_2-assist batteries, metal–CO_2 batteries currently show the most potential due to the use of active metals, such as lithium, sodium, zinc, magnesium, and aluminum, as anodes. Li–CO_2 batteries are first reported, thus providing a new way of mitigating the greenhouse effect and the generation of electrical energy simultaneously. Na–CO_2 batteries were developed later, but their high energy density and cheap cathode materials always attracted considerable attention.

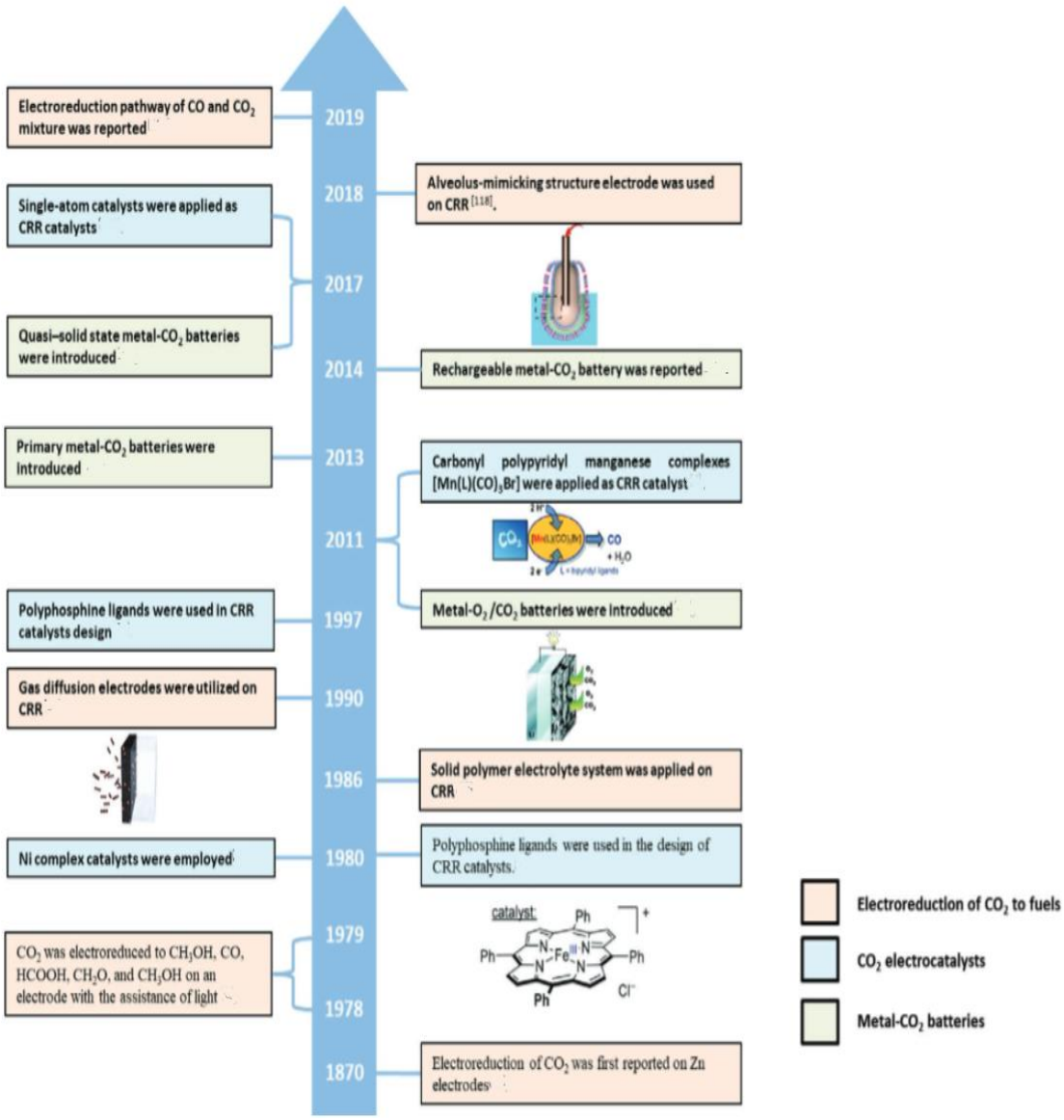

Figure 18: Milestone for the CO_2 electroreduction [92]

Thermodynamics of reduction

Electrochemical reduction of CO_2 leads to a variety of products, which depend mainly on the cathode electrode material and the electrolyte composition. The main products of electrocatalysis include HCOOH, CO, CH_4, C_2H_4, CH_3OH, $H_2C_2O_4$, CH_3CH_2OH, etc.

Kuhl's research group[93] report that electrochemical reduction of CO_2 in copper cathodes and a wide range of cathodic potential (-0.6 to -1.2 V) gave a total of 16 different reduction products (CH_3OH, CO, CH_4, acetic acid, acetaldehyde, ethanol, ethylene glycol, allyl alcohol, propionaldehyde, 1-propanol, glyoxal, glycolaldehyde, ethylene glycol, hydroxy acetone, and acetone). The equilibrium potential for the formation reaction of a reduction product depends on the pH according to Nernst equation.

$$xCO_2 + mH^+ + ne^- \leftrightarrow Product + nH_2O$$

$$E = E^o + 0.0591pH, T = 298.15\ K$$

The normal potential E^o is calculated from the Gibbs free energy according to equation:

$$E^o = -\frac{\Delta G^o}{nF}$$

In the last equation, ΔG^o is the difference of free energy, n refers to the number of electrons that take part in the formation of each product and F is the Faraday constant. Table 2 shows the normal equilibrium potentials of the reduction products. As shown in the same table, the standard redox potentials for different electron pathways have no obvious laws. This is because the whole CRR reaction process is complicated, generally containing three steps:

i) the adsorption of CO_2

ii) the surface diffusion of CO_2 and the electron and proton transformation on CO_2

iii) the desorption of products.

Table 2: Standard potential of different CO_2 electroreduction reactions [92]

Half-electrochemical thermodynamic reactions	Electrode potentials (V vs SHE) under standard conditions
$CO_2(g) + e^- = CO_2^{\cdot -}(aq)$	–1.990
$CO_2(g) + 2H^+ + 2e^- = HCOOH(l)$	–0.250
$2CO_2(g) + 2H^+ + 2e^- = H_2C_2O_4(aq)$	–0.500
$CO_2(g) + 2H_2O(l) + 2e^- = HCOO^-(aq) + OH^-$	–1.078
$2CO_2(g) + 2e^- = C_2O_4^{2-}(aq)$	–0.590
$CO_2(g) + 2H^+ + 2e^- = CO(g) + H_2O(l)$	–0.106
$CO_2(g) + 2H_2O(l) + 2e^- = CO(g) + 2OH^-$	–0.934
$CO_2(g) + 4H^+ + 4e^- = C(s) + 2H_2O(l)$	0.210
$CO_2(g) + 2H_2O(l) + 4e^- = C(s) + 4OH^-$	–0.627
$CO_2(g) + 3H_2O(l) + 4e^- = CH_2O(l) + 4OH^-$	–0.898
$CO_2(g) + 6H^+ + 6e^- = CH_3OH(l) + H_2O(l)$	0.016
$CO_2(g) + 5H_2O(l) + 6e^- = CH_3OH(l) + 6OH^-$	–0.812
$CO_2(g) + 8H^+ + 8e^- = CH_4(g) + 2H_2O(l)$	0.169
$CO_2(g) + 6H_2O(l) + 8e^- = CH_4(g) + 8OH^-$	–0.659
$2CO_2(g) + 12H^+ + 12e^- = CH_2CH_2(g) + 4H_2O(l)$	0.064
$2CO_2(g) + 12H^+ + 12e^- = CH_3CH_2OH(l) + 3H_2O(l)$	0.084
$2CO_2(g) + 9H_2O(l) + 12e^- = CH_3CH_2OH(l) + 12OH^-$	–0.744

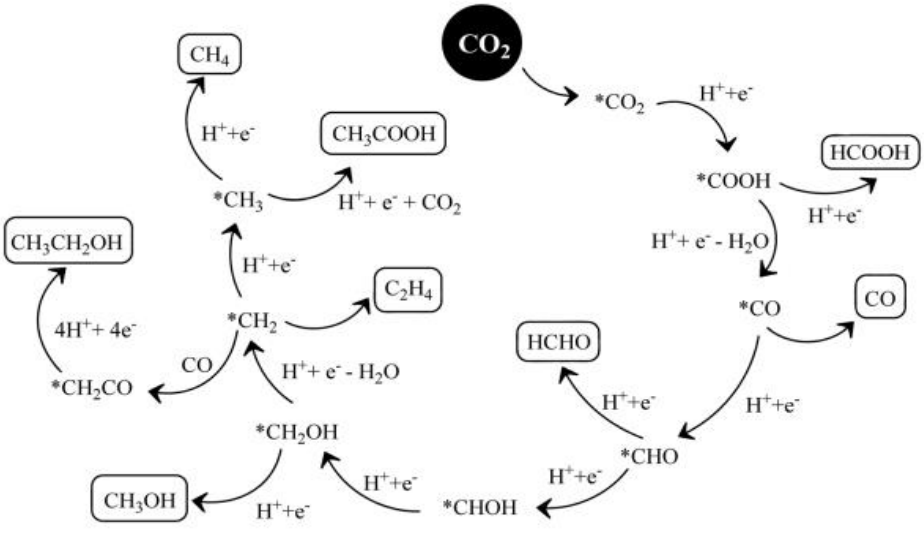

Figure 19: Various products formed due to multi-step processes during electrochemical CO_2 reduction [94]

Hydrogen Evolution Reaction (HER)

The most important competitive reaction of CO_2 reduction is the release of hydrogen (HER) that takes place in aqueous solutions. HER is one of the most studied reactions in electrochemistry.[95] Its mechanism and the speed of its conduct vary significantly, depending on the nature of the electrode. In high voltage electrodes for the release of hydrogen, the reaction is very slow and is carried out with high overpotential, while at other electrodes such as Pt, Ir, Rh, etc., the reaction is very fast and is carried out with low hypertension. At a Pt electrode, the reaction is carried out practically without hypertension.

Typically, the HER follows the Volmer-Heyrovský-Tafel mechanism[96,97] where a proton is first adsorbed into the surface of the catalyst and then reduced and releases hydrogen. The basic equation for the hydrogen evolution reaction is the following:

$$H_{2(g)} \leftrightarrow 2H^+ + 2e^-$$

This reaction comprises two intermediate steps:[98] The first step involves the uptake of an electron by a proton in acidic aqueous solutions, during the reaction:

$$M + H_3O^+ + e^- \leftrightarrow MH_{ads} + H_2O$$

or from a molecule of water in alkaline or neutral solutions, according to the reaction:

$$M + H_2O + e^- \leftrightarrow MH_{ads} + OH^-$$

while the formed atomic hydrogen is adsorbed to active positions on the electrode surface. This step of charge transfer and simultaneous adsorption of hydrogen to active positions on the electrode surface is called the Volmer reaction.

The second stage involves the desorption of hydrogen in its gaseous molecular form, from the surface of the electrode. This step can be done in one of the following two ways:

- The adsorbed hydrogen atoms diffuse over the surface of the electrode, join to form a hydrogen molecular gas, according to the following reaction. This step is called the Tafel reaction. If this reaction follows the Volmer reaction, then the total hydrogen release effect follows a Volmer-Tafel mechanism.

$$2MH_{ads} \leftrightarrow 2M + H_{2(g)}$$

- Adsorbed hydrogen atoms with simultaneous uptake of protons and electrons can give molecular hydrogen gas, according to the following reaction called Heyrovský reaction. In this case the overall phenomenon follows the mechanism called Volmer – Heyrovský.

$$MH_{ads} + H_3O^+ + e^- \leftrightarrow M + H_2O + H_{2(g)}$$

The Volmer heterogeneous electrochemical reaction is a common stage in both above mechanisms and explains the role of surface adsorption in kinetics and process mechanism, as well as the dependence of kinetics on the nature and electrocatalytic properties of the electrode. When the CO_2 is reduced to an aqueous electrolyte, the hydrogen evolution reaction competes with the reduction. This is because hydrogen production is faster and protons are adsorbed to the surface of the catalyst before carbon dioxide, thus reducing the active surface of the catalyst for further reduction of CO_2.[99]

2.3 Catalysts

Catalysis plays a vital role in our daily life. Various types of catalysts have been reported for the conversion of waste into useful products. Numerous metals have been heavily studied during the 1980s and they have been roughly grouped depending on their major reduction product.[100]

Efficiency and selectivity of a catalyst depend on a large number of factors, such as composition, crystal structure, microstructural features (surface roughness, grain/ nanoparticle size, morphology), as well as presence and number of defects (point defects, impurities, uncoordinated sites, grain boundaries).[101] It should be noted that, all these relevant properties could potentially vary under operation, thus highlighting the relevance of in situ studies. An important, additional aspect is the reductive stability of the catalysts, which is also related, particularly in aqueous systems to the pH of the electrolyte. Indeed, there is an active ongoing discussion on the identification of metal oxidation states during CO_2RR, with some metals believed to be fully reduced and some to be still partially oxidized.[102]

As mentioned before, the redox potentials can be determined by many parameters, such as the electrolyte salts, CO_2 pressure, and the types of catalysts. For example, due to generation of thermodynamically unstable products, single electron transfer requires more overpotential than proton-couple multielectron transfer. It is necessary to overcome high energy barrier of adsorbing CO_2 and forming CO_2^- anion radical. Therefore, catalysts play an important role in

facilitating the reaction rate and decreasing energy gaps. Remarkable CO2RR catalysts should possess six key traits as indicated in Figure 20.

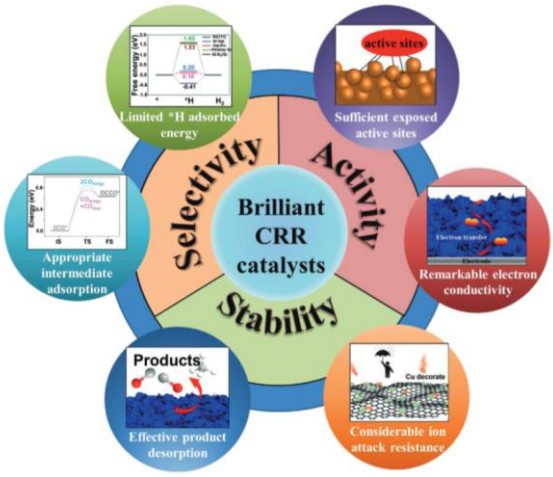

Figure 20: The traits an excellent catalyst should have[92]

MOFs as catalysts

With the development of reticular chemistry, MOFs, as one of the porous, crystalline, and extended materials, have become a popular research topic. Precise and molecular-level control is easily conducted for MOF synthesis through molecular and framework chemistry. Unsaturated metal sites play a vital role because they endow MOFs with remarkable CO_2 adsorption at low pressure. However, the competition of water molecules on the unsaturated metal sites reduces CO_2 uptake, which is an intractable challenge to deal with.

The Hinogami group first applied MOFs as electrocatalysts to reduce CO_2. They synthesized copper rubeanate MOF (CR-MOF), and its major product was formic acid. CR-MOF exhibited 0.2 V more positive onset potential and a larger yield of formic acid compared with the Cu electrode. CR-MOF showed slightly weak CO_2 adsorption and led to the high selectivity of formic acid up to 98% due to the ionic metallic site and low density of CR-MOF. However, effectively controlling pore size must still be comprehensively explored.[103]

Cu-MOF also showed considerable CO_2 capture capability and increased CO_2 concentration in aqueous solution. The entire electrode displays marked improvement of methane Faradaic efficiency from 2.5% to 20% at −1.8 V versus SCE compared with blank gas diffusion electrode (GDE) with the introduction of Cu-MOF into GDE. However, the weight ratio of Cu-MOF would effectively be controlled under 10% because additional Cu-MOF decreased GDE active sites and provided extra carbon sources for HER.

Although MOF possesses numerous merits, this framework also has defects in poor electron-donating capability and electrical conductivity. Herein, in addition to the metal center, ligand doping also plays a key role in CRR catalysis. The synergetic effect of ligand and C atoms on MOF is crucial to the enhancement of MOF catalytic capacity, especially when the metal center is not an ideal electron donor. Dou et al. reported that 1,10-phenanthroline-doped Zn-based MOFs of zeolitic imidazolate framework-8 (ZIF-8) possessed high CO Faradaic efficiency of up to 91%.

EXPERIMENTAL

3. MOFs Synthesis and Characterization

Materials and Methods

All materials were kindly offered by the Laboratory of Inorganic Materials and the partner group of Functional Materials of the Clausthal Centre of Materials Technology of the Technische Universität Clausthal, Germany. In Table 3 all used materials are presented.

Table 3: Materials used in the present work

Compound Name	Formula	Vendor	Purity (%)
Solids			
1,3,5-Benzenetricarboxylic acid	$C_9H_6O_6$	Alfa Aesar	98
2,5-Dihydroxyterephthalic acid	$C_9H_8O_4$	Sigma-Aldrich	98
2-Methylimidazole	$C_4H_6N_2$	Alfa Aesar	97
4,4-Bipyridine	$C_{10}H_8N_2$	Alfa Aesar	98
Cobalt (II) Nitrate hexahydrate	$Co(NO_3)_2{\cdot}6H_20$	Honeywell	98
Copper (II) Chloride dihydrate	$CuCl_2{\cdot}2H_2O$	Sigma-Aldrich	≥ 99
Nickel (II) Nitrate hexahydrate	$Ni(NO_3)_2{\cdot}6H_2O$	Honeywell	≥ 97
Zinc Nitrate hexahydrate	$Zn(NO_3)2{\cdot}6H_2O$	Sigma-Aldrich	98
Zinc Oxide	ZnO	Merck	≥ 99
Zirconium (IV) Oxide Chloride Octahydrate	$Cl_2OZr{\cdot}8H_2O$	Merck	99
Sodium Bicarbonate	$NaHCO_3$	Mallinckrodt	99.7-100.3
Liquids/Solvents			
Acetone	C_3H_6O	Sigma-Aldrich	≥ 99.5
Aniline	C_6H_7N	Sigma-Aldrich	≥ 99.5
Sulfuric Acid	H_2SO_4	Merck	95-97
Ethanol absolut	CH_3CH_2OH	Honeywell	≥ 98
Formic Acid	HCOOH	Merck	98-100
Methanol	CH_3OH	Chem-Lab	> 99.8
N,N-Dimethylformamide (DMF)	C_3H_7NO	Chem-Lab	> 99.5
Triethylamine (TEA)	-	Sigma-Aldrich	≥ 99.9

The MOFs were synthesized via sonochemical and/or solvothermal route. They were basically characterized via X-Ray Diffraction (XRD). Finally, some of the samples were also characterized by Scanning Electron Microscopy (SEM).

The sonochemical synthesis was conducted with the use of sonicator Vibra Cell VCX 750 W (20kHz) [d=13 mm].

X Ray Diffraction was carried out at Chemical Engineering Department with a Bruker D8 Advance diffractometer with a Cu K_a radiation (λ=1.5406 ˚A) at 40kV and 40mA with a step of 0.05° at 2θ. All the reference patterns have been obtained from Cambridge Crystallographic Data Centre.

Synthesis

The synthesized MOFs are going to be presented in series, based on the metal part. As a result, there are Ni-series, Cu-series, and Zn-series.

Cu-series

HKUST – 1_ST

1:1 molar ratio of H_3BTC and $CuCl_2 \cdot 2H2O$ (0.6315g,3mmol and 0.5152 g,3 mmol respectively) were dissolved in 50ml mixed solvent of deionized water: EtOH :DMF = 1:1:1 v/v. The solution was transferred into a to a glass bottle, sealed with a screwed cap and maintained at 110 °C for 24h in convection oven. The resulting blue crystals were thoroughly washed several times with DMF and ethanol. Finally, it was left to dry at 100 °C for 24h.[104]

HKUST – 1_US

$CuCl_2 \cdot 2H_2O$ and H_3BTC at one-to-one molar ratio were dissolved under magnetic stirring in a mixture of solvents DMF: EtOH: deionized water, 30:15:30 v/v respectively. Then, the solution was transferred to a three-neck round bottom flask (100 ml) and sonicated at 65% power for 1h.

When the reaction was finished, the mixture was left to cool down at room temperature. The formed precipitate was centrifugated several times with DMF, EtOH and deionized water. Finally, the solution was transferred into a to a glass bottle, sealed with a screwed cap and dried out at 100 °C overnight.

Cu/PANI – BTC_ST

In an effort to use MOF composites for electrochemical experiments, Cu/PANI MOF was fabricated by a two-step process including the chemical polymerization of aniline.[105]

Synthesis of Polyaniline: About 25 mL of H_2SO_4 (2 M) was mixed with 4.5 mL of aniline monomer in 100 mL distilled water and stirred for 2 h in the ice bath. Subsequently, 50 mL ammonium persulfate (0.25 M) was added slowly during 1 h while stirring. After 4 h of stirring in the ice bath, the precipitate was aged for 24 h and then was filtered off, washed with distillated water and EtOH, and finally dried in the oven with 60 °C for 12 h.

The PANI/Cu-MOF composite was prepared as follows: H_3BTC (0.256 g, 1.5 mmol) and $CuCl_2 \cdot 2H_2O$ (0.315 g, 1.5 mmol) were dissolved in a mixed solvent of EtOH :DMF :deionized water (20:20:20ml) with 1:1:1: volume ratio. Then, 0.047 g of polyaniline were suspended in the above-mentioned mixed solvent with ultrasonic irradiation for 80 min (30%). The copper

solution was added to the polyaniline mixture and irradiated for 1 h. 0.315 μL of triethylamine were added and the resulting mixture was stirred for 24 h at room temperature. Afterwards, the dark blue crystals were centrifuged, washed with distillated water and methanol, and dried in the oven with 110 °C for 24 h.

Due to the different precursors from the original experiment in literature, the appropriate adjustments have been made.

Ni-series

Ni-BTC_ST

For this sample $Ni(NO_3)_2 \cdot 6H_2O$ and H_3BTC were used as precursors at 1:1 molar ratio. 0.4418 gr of the metal salt and 0.3183 gr of the linker were dissolved in 50ml mixed solvent of deionized water: EtOH :DMF = 1:1:1 v/v. The solution was transferred to a glass bottle, sealed with a screwed cap and stayed for 24h at 110 ^oC in convection oven to dry. The green crystals formed were washed several times with DMF and EtOH and dried overnight at 90 ^oC.[106]

Ni-BTC-bpy_ST

Precursors $Ni(NO_3)_2 \cdot 6H_2O$ as metal salt and H_3BTC and 4,4 Bipyridine as linkers (1:1:1 molar ratio, 0.4358 gr metal salt, 0.3153 gr and 0.2346 gr respectively) were used for the fabrication of this material. The precursors were dissolved in 60 mL DMF with stirring at room temperature. Then, the resulting mixture was transferred to a glass bottle, sealed with a screwed cap and left to dry in convection oven for 18 h at 80 ^oC. The formed precipitation was thoroughly washed with DMF and EtOH followed by a drying step overnight at 110 ^oC.

Ni-BTC-bpy_US

The exact same precursors, solvent and quantities as in the before mentioned solvothermal route were used for the sonochemical synthesis of this material. This time, the resulting mixture was transferred to a three-neck round bottom flask (100 mL) and sonicated at 40% power for 1h. Right after the cooling in room temperature the resulting precipitate was thoroughly washed several times with DMF and EtOH. Finally, it was transferred to a glass bottle, sealed with a screwed cap and dried out in convection oven overnight at 110 ^oC.

Zr-series

MOF-808_ST

H_3BTC and $Cl_2OZr{\cdot}8H_2O$ at one-to-one molar ratio (0.11 gr and 0.16 gr respectively) were dissolved in a solvent mixture of DMF and formic acid (1:1 v/v, 40 mL each) were placed in a 60-mL screw capped glass bottled. Then the solution was heated to 100 °C for 7 days in convection oven. The colorless precipitated crystals were collected and washed with DMF and acetone. Finally, the resulting crystals were dried overnight 130 °C.[107]

MOF-808_US

The sonochemical route involved a three-neck round bottom flask, where H_3BTC and $Cl_2OZr{\cdot}8H_2O$ (1:1 molar ratio, 0.11 gr and 0.16 gr respectively) were dissolved in DMF and formic acid at 1:1 v/v (80ml total volume). The solution was sonicated for 1h at 40% power. The formed precipitation was collected and washed with DMF and acetone. Finally, the resulting colorless precipitation was transferred to a glass bottle, sealed with a screwed cap and dried out in convection oven overnight at 90 ^{o}C.

Zn- series

MOF-74_ST

MOF-74 with Zinc was fabricated by adding 0.48 gr (0.5mmol) $Zn(NO_3)_2{\cdot}6H_2O$ and 0.099 gr (0.5 mmol) 2,5-Dihydroxyterephthalic acid to a mixed solvent of DMF, EtOH and deionized water (30:2:2 ml). The mixture was then transferred to a glass bottle, sealed with a screwed cap, and placed in convection oven at 125°C for 24 h. Afterwards, the precipitation was washed with methanol and finally, dried out at 110°C overnight.

MOF-74_US

The sonochemical synthesis of MOF-74 was carried out at a three-neck round bottom flask, where 2,5-Dihydroxyterephthalic acid and $Zn(NO_3)_2{\cdot}6H_2O$ (0.949 mmol - 0.188 gr and 3.14 mmol - 0.934 g respectively) were dissolved a mixed solvent of DMF, EtOH and deionized water (30:2:2 ml). The resulting mixture was sonicated for 1 h at 65% power. It is left to cool down at room temperature and then, centrifugated several times with DMF and MeOH. The resulting solid was activated under vacuum at 250°C for 12h.

ZIF-8_RT

In this experiment, ZIF-8 was synthesized in room temperature under continuous magnetic stirring. $Zn(NO_3)_2{\cdot}6H_2O$ (3.75 mmol, 1.116 gr) and 2-Methylimidazole (15 mmol, 1.235 gr) were dissolved in 60 ml MeOH. The solution was transferred to glass jar and vigorously stirred under

magnetic assistance for 17 h. The precipitation was collected, centrifugated with MeOH and finally, dried overnight at 90°C.

ZIF-8_ST

The typical solvothermal synthesis of ZIF-8 involves the one-to-one molar ratio of $Zn(NO_3)_2 \cdot 6H_2O$ (1.2 mmol, 0.3648 gr) and 2-Methylimidazole (1.2 mmol, 0.098 gr). The reactants were dissolved in DMF, transferred to a sealed glass bottle, and remained at 140°C in convection oven for 24h. The precipitation was washed several times with DMF and MeOH respectively and dried at 110°C overnight to obtain the final crystals.

ZIF-8_US

For the sonochemically synthesized ZIF-8 0.5895 gr of the metal salt $Zn(NO_3)_2 \cdot 6H_2O$ and 0.1642 gr of the linker 2-Methylimidazole (1:1 molar ratio) were dissolved in DMF with the addition of 0.5 ml TEA. The mixture was transferred in a three-neck round flask and sonicated for 1 h at 40% power. After cooling at room temperature, the mixture was centrifugated with DMF and MeOH. Finally, it was transferred to a glass bottle, sealed with a screwed cap and placed in convection oven at 110 °C for 24 h to dry.

ZIF-8_CALCINATED

The ZIF-8 fabricated in room temperature under magnetic stirring was calcinated at 500°C for 2h to obtain ZnO.

X Ray Diffraction

As illustrated in the Figure 21, the simulated and the experimentally synthesized HKUST – 1 are identified. As a result, it is safe to mention that the both lab fabricated solvothermally and sonochemically HKUST-1 are in accordance with the literature.

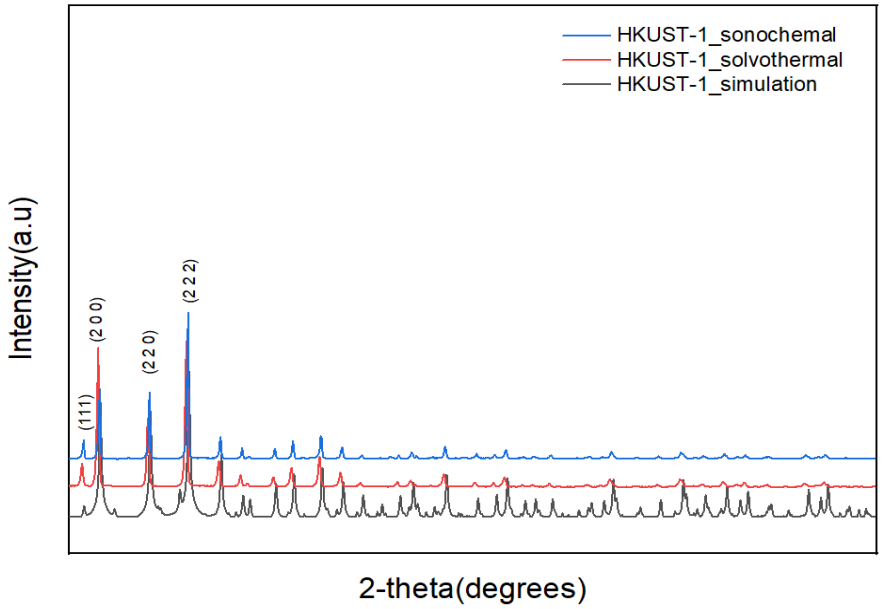

Figure 21: XRD pattern of the simulated and the synthesized HKUST -1

The experimental Cu/PANI MOF appears to have the same peaks as the simulated, so it was successfully synthesized (Figure 22).

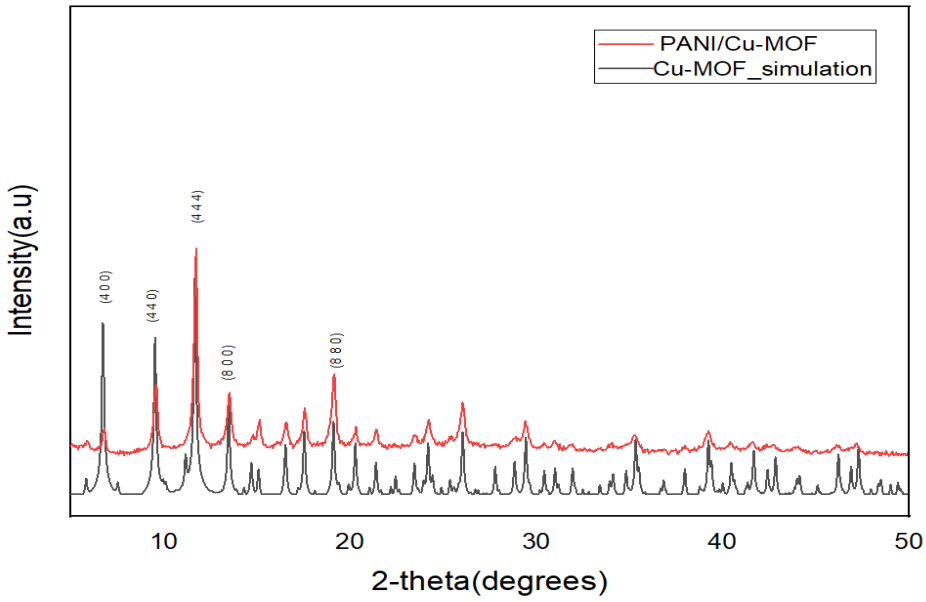

Figure 22: XRD pattern of the simulated and the synthesized Cu/PANI MOF

As far as the Ni-BTC MOF is concerned, the XRD pattern obtained from literature is not in accordance with the one fabricated in the lab, as shown in Figure 23. This leads to the result that the solvothermally synthesized MOF has not the same structure as the simulated, as it was originally targeted; yet further investigation is required.

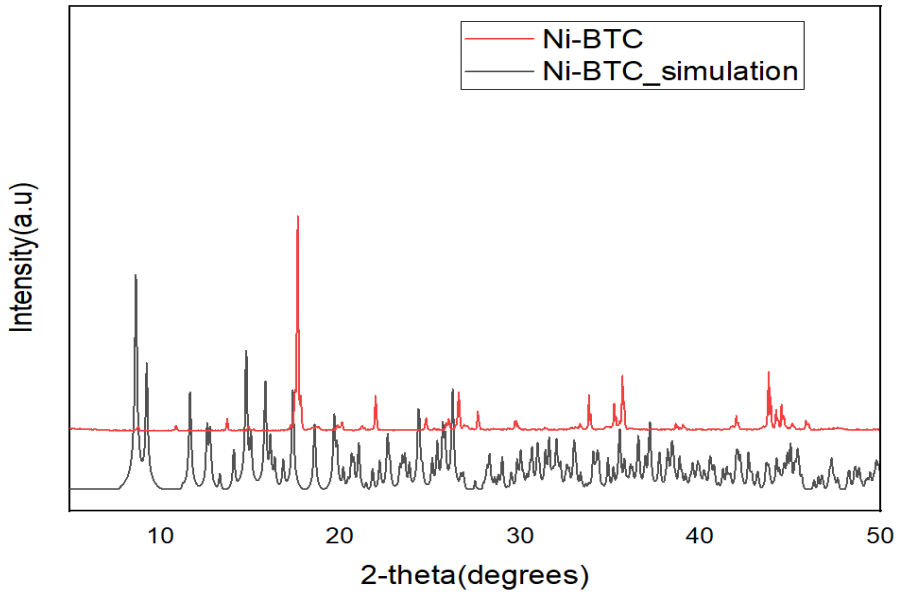

Figure 23: XRD pattern of the simulated and the synthesized Ni – BTC MOF – There are no common peaks between the simulated Ni-BTC and the as synthesized material

In the following figure (Figure 24), the XRD pattern of the simulated Ni-BTC-bpy MOF and the experimental solvothermally and sonochemically synthesized Ni-BTC-bpy MOFs are presented. The fabricated materials are in accordance with literature.

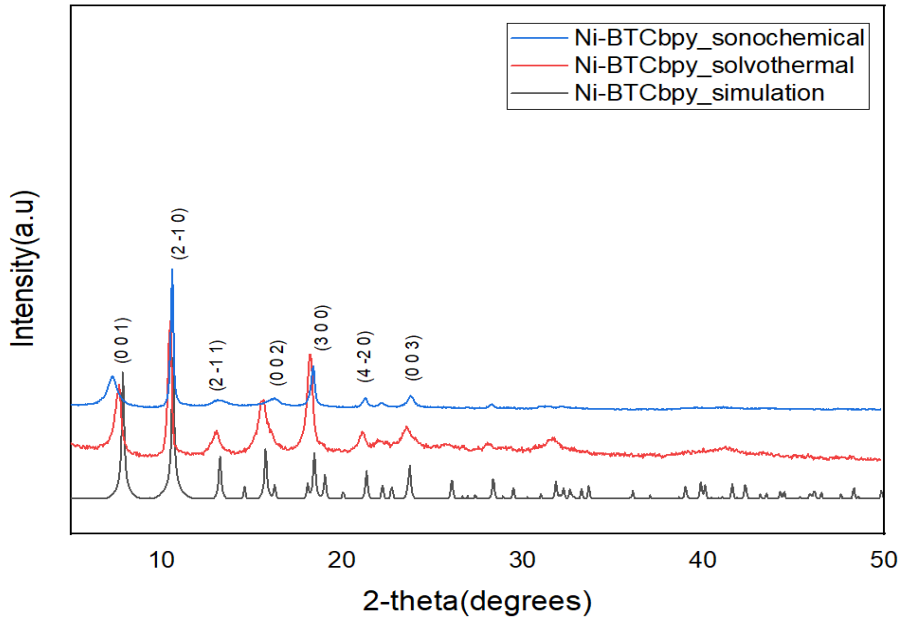

Figure 24: XRD pattern of the simulated Ni-BTC/Bpy and the synthesized solvothermal and sonochemical materials. The peaks do not assemble, so it is not certain that the as synthesized materials are Ni-NTC/Bpy

As far as MOFs-808 are concerned, the XRD patterns are illustrated in Figure 25. In this case there is agreement between the simulated and the experimentally synthesized MOFs. Both solvothermal and sonochemical MOFs present the same peaks as the simulated one, as a result there is certainty that the as mentioned materials are successfully fabricated in the lab.

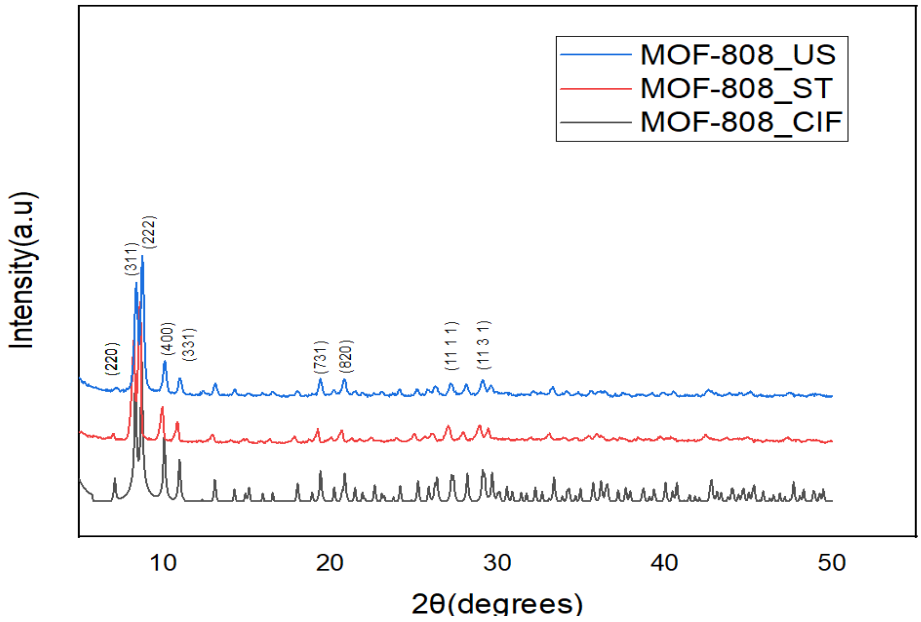

Figure 25: XRD pattern of the simulated and the synthesized MOFs 808

Most of the peaks that appear in the experimental MOF-74 are identified with the simulated, as shown in Figure 26.

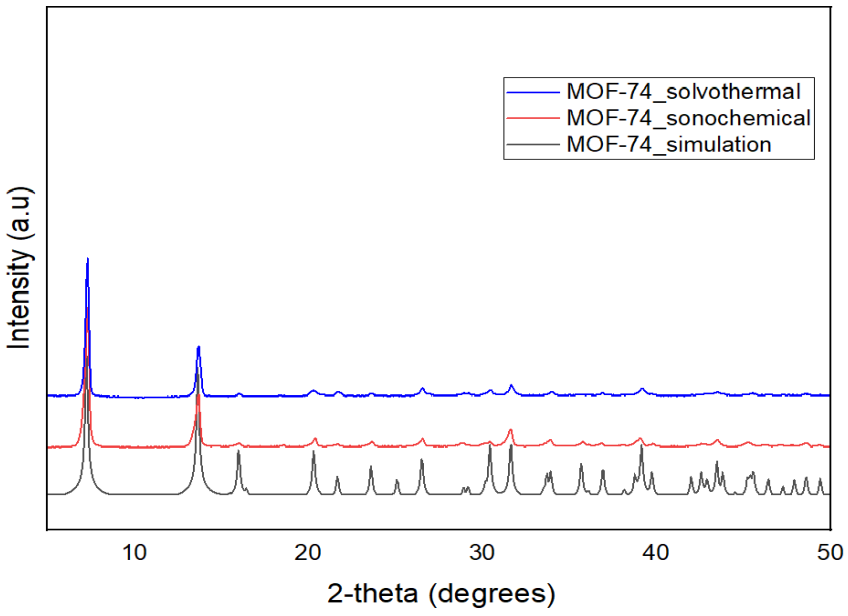

Figure 26: XRD pattern of the simulated and the synthesized MOF-74

Regarding the ZIFs, all three synthesis, solvothermal,sonochemical,and stirring in room temperature are successful and in accordance with the simulation, as presented in Figure 27.

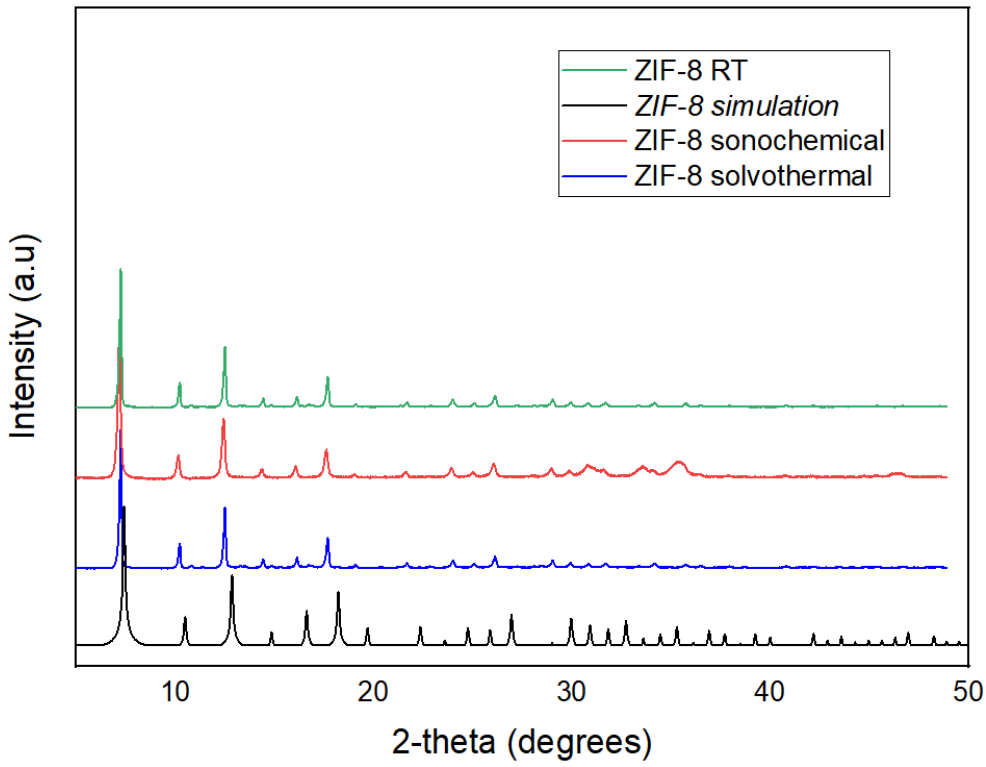

Figure 27: XRD pattern of the simulated and the synthesized ZIF-8

As far as the zinc oxides are concerned, the commercial and the derived from ZIF-8_RT present the same peaks. It is should be noted though, that the derived presents more noise, as illustrated in Figure 28.

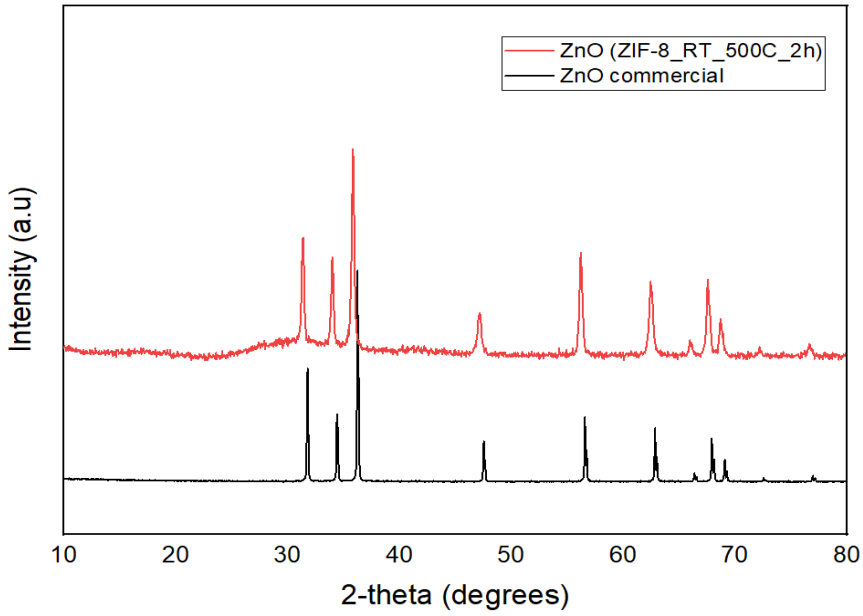

Figure 28: XRD pattern for ZnO, commercial and derived from ZIF-8_RT

Scanning Electron Microscopy

These characterization experiments were conducted with Zeiss Supra 55 and Hitachi SU-70.

Firstly, the SEM images for HKUST-1 samples are illustrated in Figures 29 and 30. HKUST-1_ST presents no uniformity in size and shape, with an average crystal size of 50 μm. The sonochemical HKUST-1 as shown in Figure 30, also presents inhomogeneity in size and shape but, the average size is less than 50 μm.

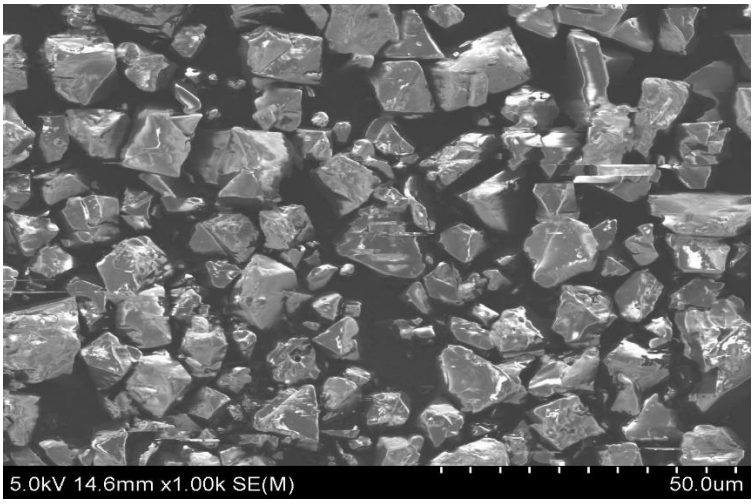

Figure 29: SEM image for the solvothermal HKUST-1

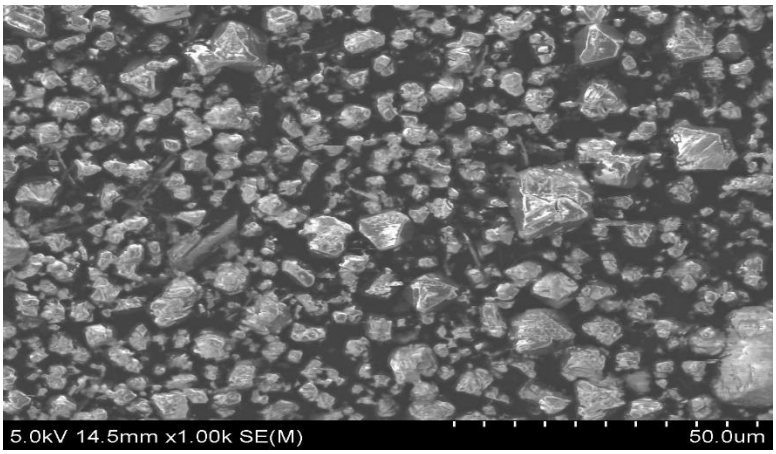

Figure 30: SEM image for the sonochemical HKUST-1

The next images, Figures 31 and 32, present Ni-BTC/bpy samples, solvothermal and sonochemical respectively. The solvothermal, as presents in Figure 31, does not show any homogeneity neither in size, nor in shape. On the other hand, in Figure 32, on the left it is

clearly presented uniformity in size for the sonochemical sample. In Figure 32 on the right, where there is higher resolution, the shape of the crystals seems as cubic.

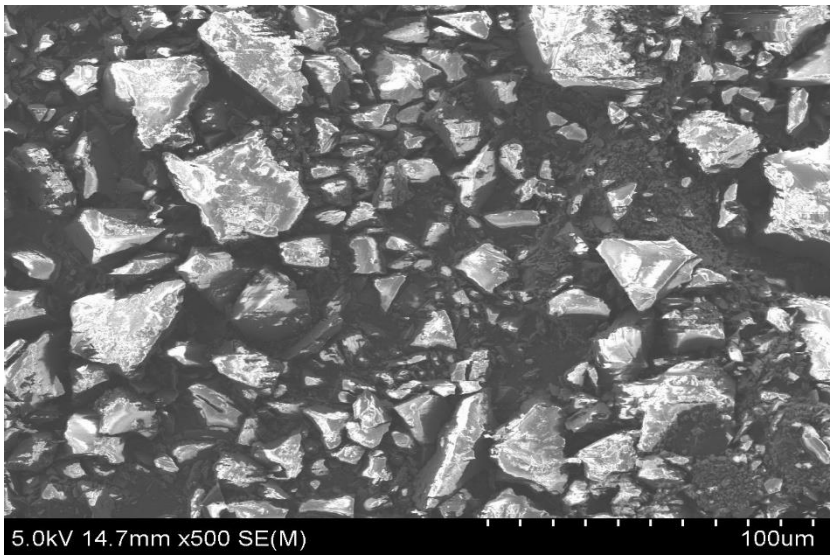

Figure 31: SEM image for Ni-BTC/bpy solvothermally synthesized

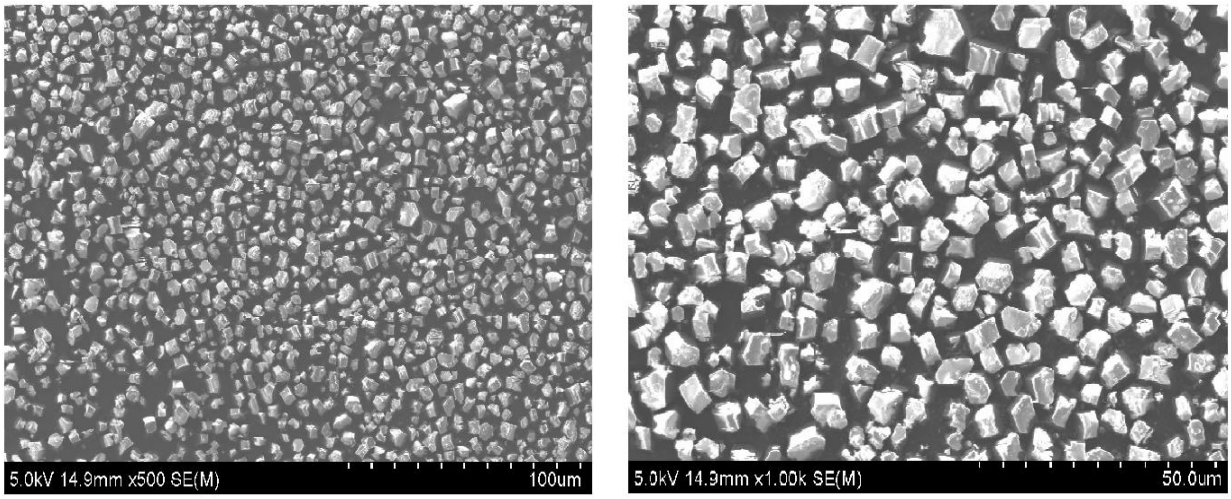

Figure 32: SEM images for Ni-BTC/bpy sonochemical in two different resolutions. Left x500 and right x1000

For MOF-808, the resulting SEM images are shown in Figure 29 and Figure 30. In Figure 29, it is reflected the microstructure of MOF 808_ST in resolution x2500 and x5000 on the left and right, respectively. First of all, it is not a nanomaterial since its crystals exceed the level of micrometers, but on the other hand it is crystalline. It seems that the structure is basically tetrahedral without the formation of aggregates. As for the sonochemical sample in Figure 30, there is no uniformity in size and shape.

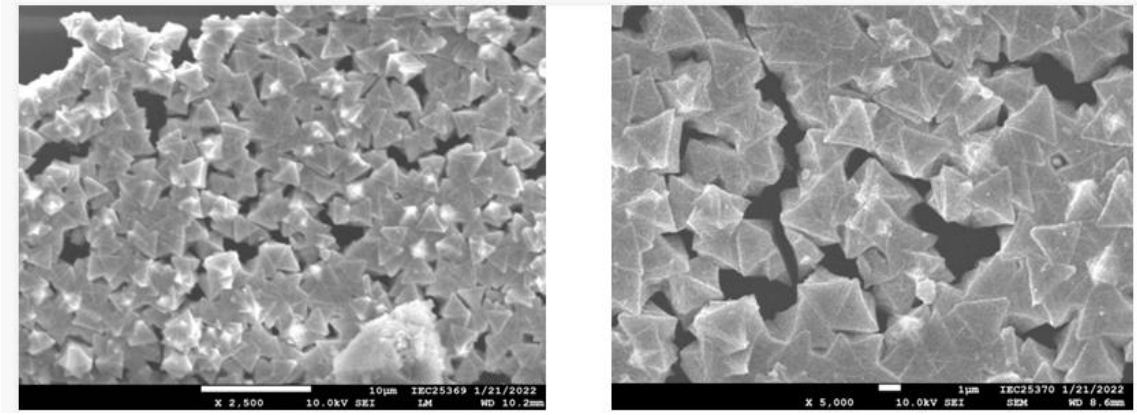

Figure 33: SEM images for MOF 808_ST. On the left resolution is x2500 and on the right x5000. On the left image tetrahedral crystals are clearly shown

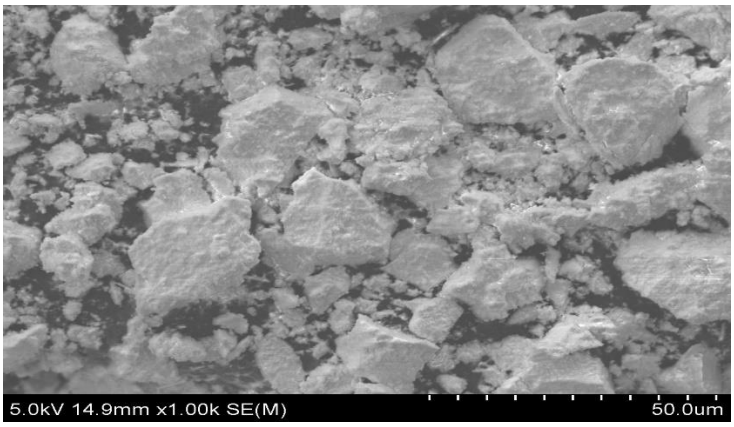

Figure 34: SEM images for MOF 808_US. As illustrated, there is no uniformity in size and shape

Figure 28 clearly illustrates the SEM images of the sonochemically synthesized MOF-74. On the right image, aggregates are present as shown, while the structure is crystalline, almost rod-like. On the left image, higher resolution allows the deduction that there is no uniformity in the size of the rods.

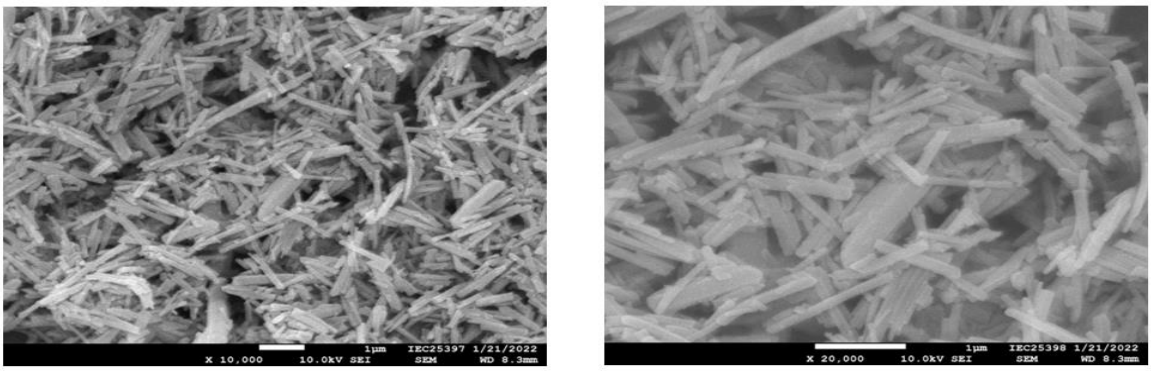

Figure 35: SEM images for MOF-74 US. On the right image it is observed aggregation, while the higher resolution of the left image illustrates the absence of size uniformity

The SEM images for ZIF-8 fabricated in room temperature with magnetic stirring are presented below (figure 29). This material seems perfectly crystalline with polyhedric crystals. There is uniformity in size, too. Finally, the crystals of this material are in the scale of nanometers as it can be seen from the right image of Figure 29.

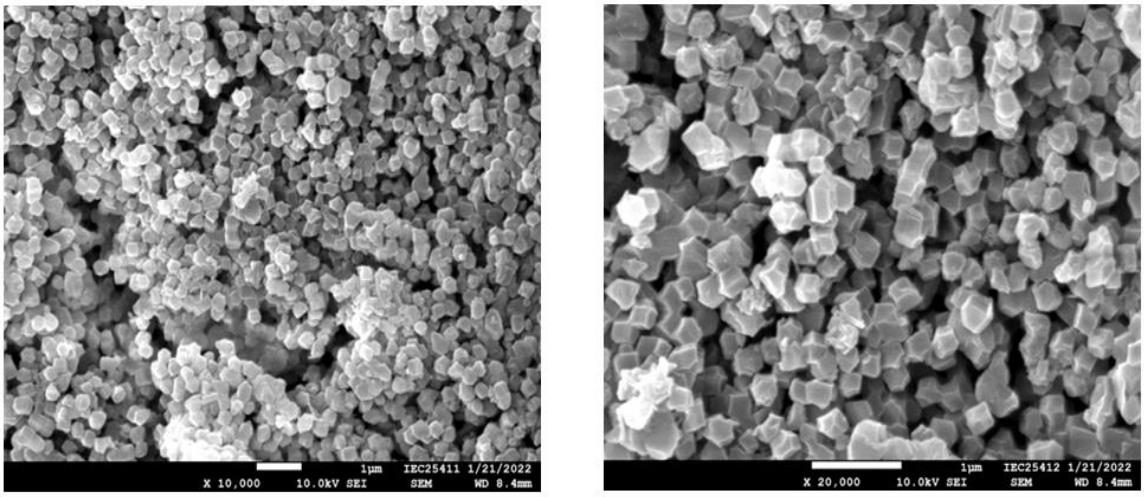

Figure 36: SEM images for ZIF-8_RT. Higher magnification on the right image (resolution x20000) reveals uniform polyhedric nanocrystals.

ZIF-8_RT is followed by the solvothermally synthesized ZIF-8. For this material the aggregates formed are clear, as illustrated in figure 30 (left, resolution x10000). The microstructure seems sheet-like and there is no uniformity in size.

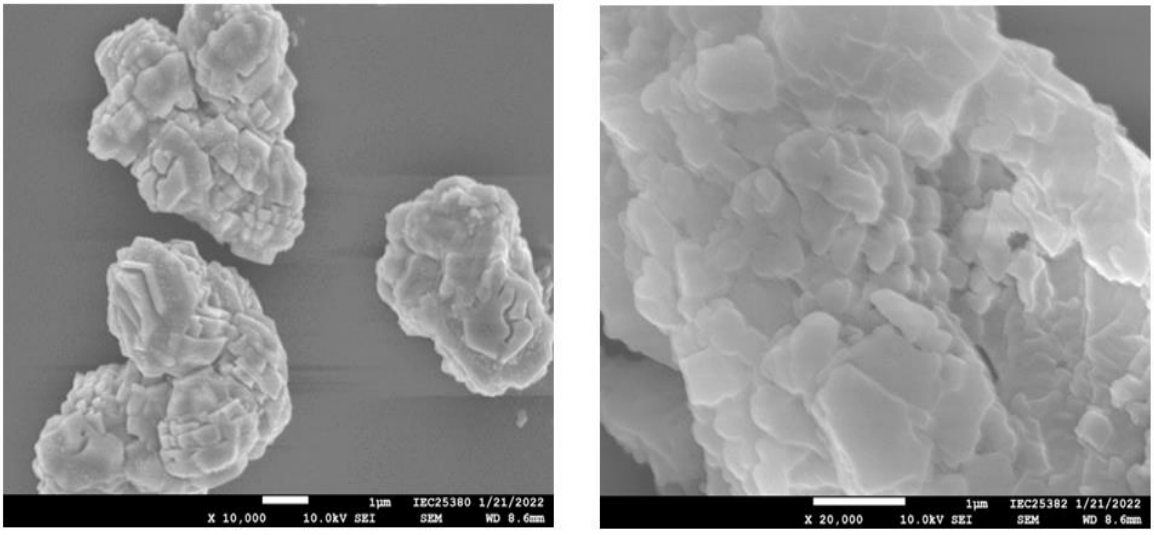

Figure 37: SEM images for ZIF-8_ST. On the left, clear aggregates are shown, while there is no uniformity in shape and size. Sheet-like crystals are assumed due to the higher resolution of the right image.

Finally, in Figure 31, the SEM image is presented for ZIF-8 sonochemically synthesized. Even though the image is not so clear, it is certain that an average crystallite size is 100 nm. On the other hand, there is no uniformity the shape of the crystals.

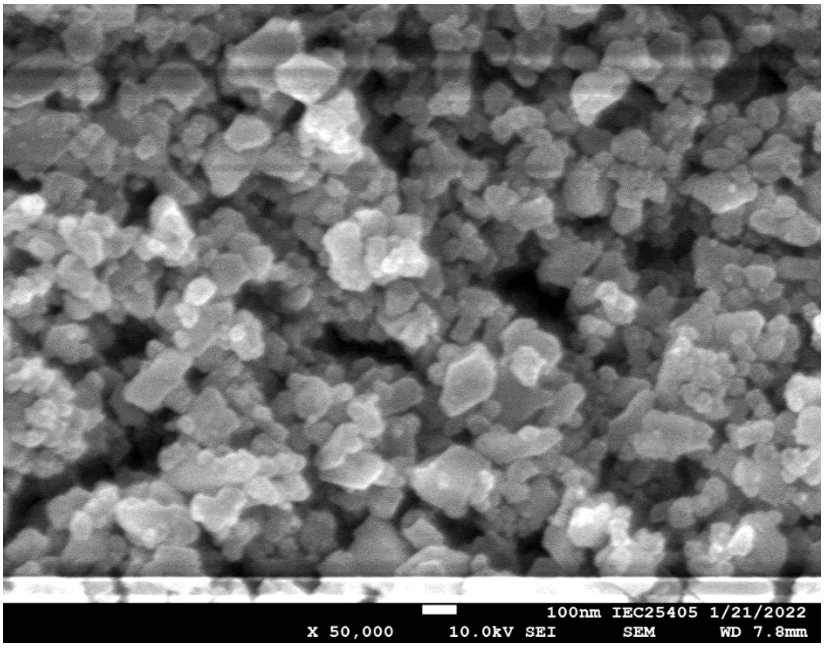

Figure 38: SEM image for ZIF-8_US. Crystals are formed, but with no uniformity in shape and size.

A general comment, regarding the ZIF series characterized by Scanning Electron Microscopy, is that the solvothermal ZIF-8 does not show strict crystallinity compared to ZIF-8 fabricated in room temperature with magnetic stirring. Moreover, the sonochemical sample illustrates absence of shape and size uniformity. All three represent differently shaped crystals, which means firstly, that more characterization methods are needed and secondly, that optimization of solvothermal and sonochemical pathways is required.

4. CO2 Reduction Experiments

Experimental Setup

The experiments were conducted in an H-type cell, as shown in Figure 32. In this setup, the working electrode, reference electrode and the counter electrode are fixed inside the two reaction chambers with the working electrode and the reference electrode being in the same cell. The chambers were separated by Nafion 117 membrane for proton exchange. Each cell was filled with 80ml of $NaHCO_3$ 0.5M, which served as electrolyte.

Carbon dioxide gas was purged into the cathode chamber and the products were inserted in gas chromatographer. At the same time, the three electrodes were properly connected to the potentiostat (Biologic SP-150) for the electrochemical measurements.

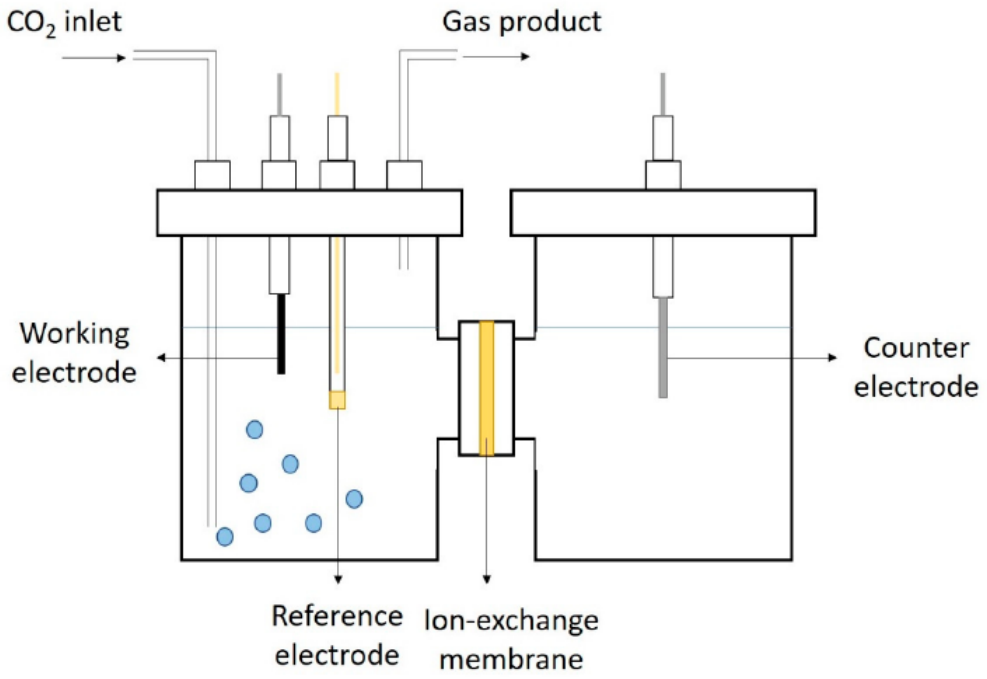

Figure 39: Schematic illustration of an H-type cell. [108]*The gas product is the inlet to the gas chromatographer. All three electrodes are connected to the potentiostat.*

The electrochemical measurements (CO_2 Reduction Reaction, CO_2RR) were carried out in a gas-tight H-type cell separated by a Nafion 117 membrane. The working electrode (WE) and reference electrode (RE) (Ag/AgCl, sat'd) are inserted in the cathode department and the counter electrode (CE) (Pt mesh) in the anode one. Both the anode and the cathode are filled with 0.5 M $NaHCO_3$ as the aqueous electrolyte. Before the experiment the cathode is purged with CO_2 for 45 min. A continuous flow of CO_2 (30 mL/min) was used throughout the

electrocatalysis and was regulated with mass flow controllers (Vögtlin Instruments). Each selected potential for the CO_2 reduction was set with a potentiostat for 30 min. The gas outlet was connected to a gas chromatographer (Bruker GC-436) equipped with a TCD and a HayesepQ column for the quantitative analysis of gas products.

Electrodes

Working Electrode Preparation

All the working electrodes (WE) were prepared as following: 5mg of the synthesized MOF were suspended in 500μl Isopropanol and were put in ultrasound bath for up to 15 minutes. Then, with the addition of 50μl Nafion solution 5% (Quintech), the slurry was left in the ultrasound bath for an hour.

The substrate for all electrodes was carbon paper of 2.5 cm^2 surface area (1cm x 2.5cm).

250μl of the MOF slurry were uniformly spread onto the substrate assisted by a micropipette and then dried under room temperature. On each electrode, the loading MOF was 1.0 mg/cm^2.

The working electrodes were serving as cathodes for CO_2 Reduction Reaction (CO2RR) to test their electrocatalytic activity measured by Faradaic Efficiency (see section *Electrocatalytic Experiment – FE Calculation*)

Reference Electrode

In all experiments the reference electrode (RE) used was saturated Ag/AgCl which is generally quite common among electrochemical experiments. It is composed of a silver wire and immersed in a solution that is saturated with potassium chloride. The actual potential of the half-cell prepared in this way is +0.197 V vs Standard Hydrogen Electrode. The pertinent half reaction is

$$AgCl_{(s)} + e^- \leftrightarrows Ag_{(s)} + Cl^-(sat'd)$$

Counter Electrode

The counter electrode in use was a commercial platinum electrode of 2.5 cm^2 surface area.

Electrolyte

As mentioned before the electrolyte was 0.5M $NaHCO_3$. The solution was made by dissolving 21gr of $NaHCO_3$ purchased by Mallinckrodt to 0.5lt of deionized water.

Electrochemical experiments

Once the setup is assembled, CO_2 purge starts in the cathode cell. At the same time, an Open Circuit Voltage (OCV) electrochemical measurement takes place. Then, the second electrochemical measurement is Linear Sweep Voltammetry (LSV) and finally, Chronoamperometry (CA) takes place as the last electrochemical measurement to check the product formation and measure current density in a standard potential.

Open Circuit Voltage (OCV)

OCV consists of a period during which no current can flow, and no potential can be applied to the working electrode. The cell is disconnected from the power amplifier.

On the cell, the potential measurement is available, so the evolution of the rest potential can be recorded. This period is commonly used as preconditioning time or for the system to reach thermodynamic equilibrium.

Linear Sweep Voltammetry (LSV)

Linear Sweep Voltammetry (LSV) is a voltametric technique used to analyze the oxidation and reduction processes occurring between a stationary working electrode (WE) and a counter electrode (CE) while using a supporting reference electrode (RE) in a three-electrode configuration. In LSV the potential scan is applied linearly versus time, in a single direction, starting from a potential where no electrode reaction is happening, to either positive potentials (oxidation) or negative potentials (reduction), while measuring the current response.[109]

For the experiments conducted of this thesis, the negative potential range was from 0 to -2.5 V versus the reference electrode.

Chronoamperometry (CA)

Chronoamperometry consists of the application of constant potential to the working electrode (WE) and the current is measured as a function of time. The current – time response reflects the change of the concentration gradient in the vicinity of the surface. It is often used to measure the diffusion coefficient of the electroactive species or the surface area of the working electrode. Also, it is used for the study of the electrode process mechanism.

An alternative and very useful way of recording the electrochemical response is to integrate the current, so that one obtains the charged passed as a function of time.

Here, chronoamperometry is applied from -1.5V to the potential that the potentionstat overloads while the current density is measured. The current is used for the calculation of Faradaic Efficiency (FE).

Electrocatalytic Experiment – FE calculation

The second basic goal of this thesis is the calculation of the Faradaic Efficiency between MOFs in order to investigate their catalytic behavior in CO2RR. Faraday's laws of electrolysis are two quantitative laws used to express the magnitudes of electrolytic effects. They were first described by the English scientist Michael Faraday in 1833.[110] The laws state the following:

The amount of chemical change produced by current at an electrode-electrolyte boundary is proportional to the quantity of electricity used, and

The amounts of chemical changes produced by the same quantity of electricity in different substances are proportional to their equivalent weights.

If the current is not constant during electrolysis, quantity of charge is calculated as the integral of the current in the axis of time.

$$Q = \int I(t)dt$$

In agreement with the mentioned above, Faradaic Efficiency can be calculated as

$$FE = \frac{n_{products}[mol\ prod] \cdot n_{e^-}\left[\frac{mol\ e^-}{mol\ prod}\right] \cdot F\left[\frac{C}{mol\ e^-}\right]}{\int_0^t Idt\ [C]}$$

Where F is the faradaic constant 96485 C/mol, $n_{products}$ is the number of moles of the formatted product, n_e is the number of electrons needed for the product formation and I is the current.

The electrocatalytic experiments of CO_2 reduction led to the formation of CO according to the following reaction

$$CO_{2(g)} + 2H^+ + 2e^- \rightarrow CO_{(g)} + H_2O_{(l)}$$

In the following section, the results of the experiments are presented for the Cu-series and the Zn-series of MOFs, starting by the Linear Sweep Voltammetry, continuing with Chronoamperometry and as a conclusion, the Faradaic Efficiency.

Cu-series

In the copper MOF series, only HKUST-1 solvothermally synthesized and Cu/PANI MOF resulted in product formation. Their LSVs are presented in the same diagram (Figure 33) creating different slopes after -1.3V.

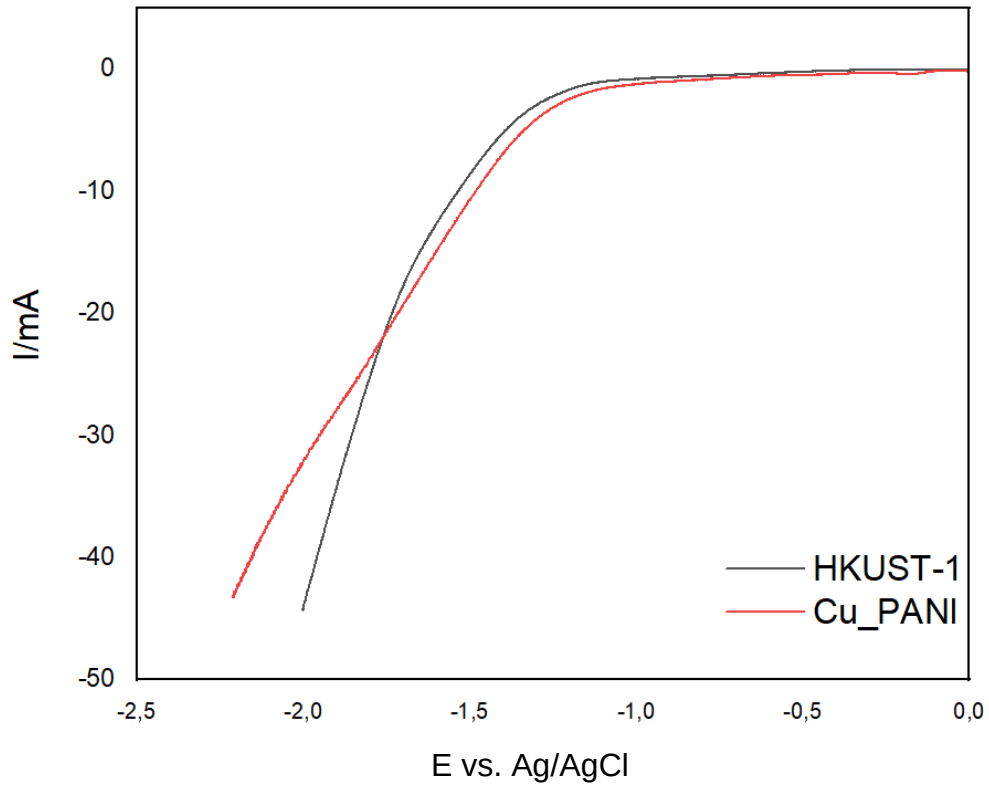

Figure 40: LSV for HKUST-1 solvothermal and Cu/PANI MOF. At ~-1.5V their slopes differ, but both MOFs reach almost -45 mA.

Regarding the CAs of these two materials, firstly both electrodes reach -1.8 V without overloading, as shown in Figures 34 and 35. Both, at -1.5 V are stable, and HKUST-1 remains stable in all measurements. Cu/PANI MOF at -1.7V starts as stable, but at 25 min creates a slope. This could be due to a human error for example, a slight movement of the electrodes. At -1.8V, HKUST-1 appears to create slope. This might be an indicator of loss of stability with time. Cu/PANI on the other hand, shows different behavior at the same voltage, with an increase in current, which remained stable during the measurement.

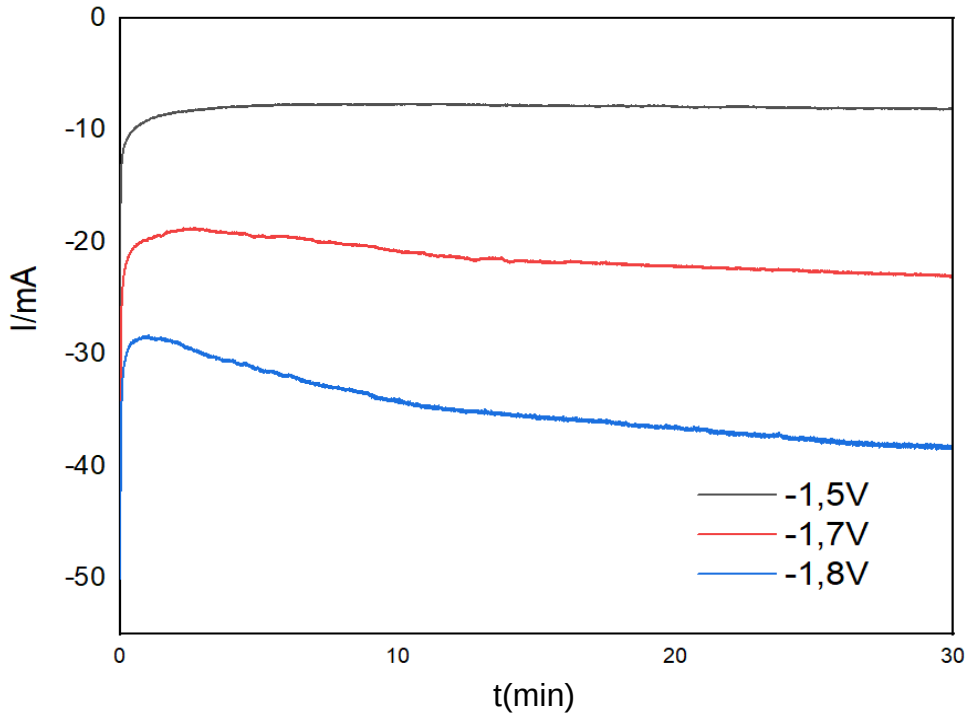

Figure 41: CA results for HKUST-1 at different potentials

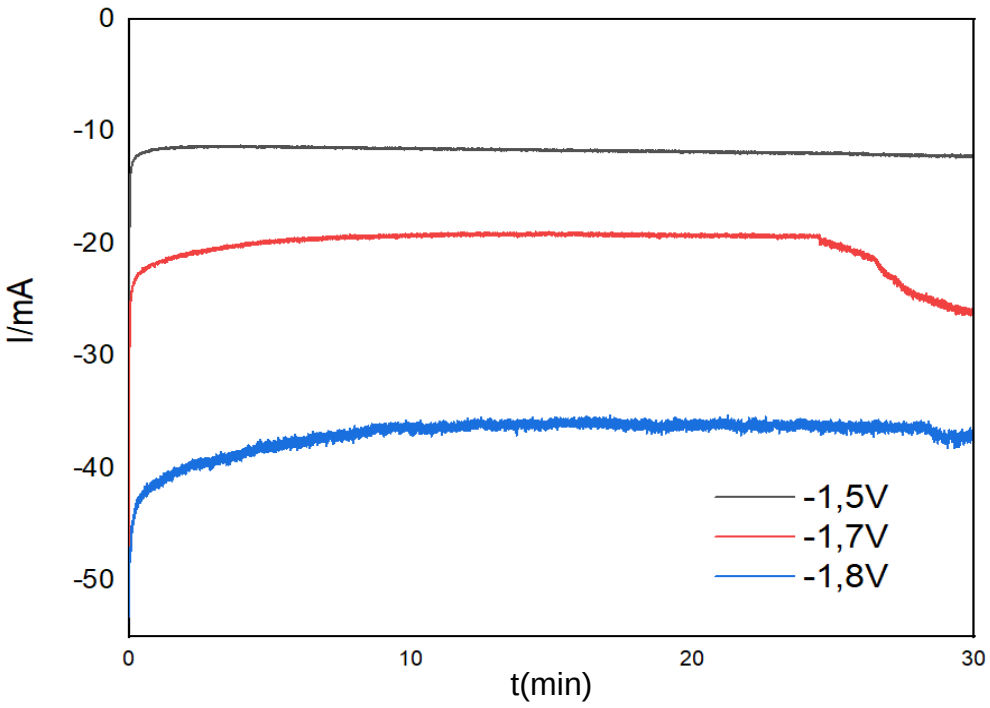

Figure 42: CA results for Cu/PANI MOF in different potentials. At -1.7V at 25 min a slope is created.

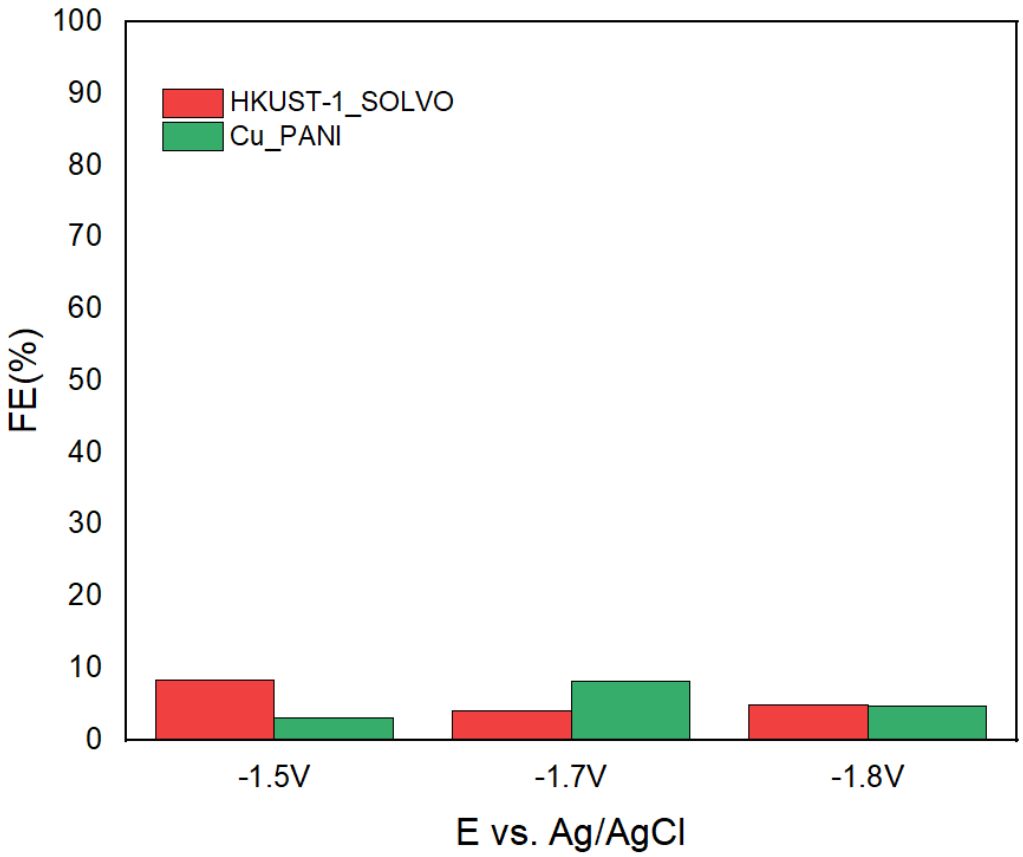

Figure 43: FE (%) comparison between HKUST-1 and Cu/PANI. At -1.8V the Faradaic Efficiency is almost the same for both materials

In Figure 36, it is illustrated the comparison between the Faradaic Efficiencies of these two materials. First of all, both do not reach 10%, which means that the quantity of the formed carbon monoxide is very low. Even though that HKUST-1 illustrates greater FE value at -1.5V, it drops in the next two experiments, remaining stable for both. Cu/PANI MOF on the other hand, has its major FE value at -1.7V, which drops at -1.8V, but it still has greater value than the first measurement at -1.5V. Both materials, appear to have almost the same FE at -1.8V.

Zn-series

MOF-74

The LSV for the MOF-74 samples, sonochemical and solvothermal, is represented in Figure 37. It is interesting to mention that here, the slope formed is around -1.2V for the sonochemically fabricated, while for the sonochemical it starts at -1.5V. The solvothermal reaches -2.2V, while the sonochemical reaches -2.05V.

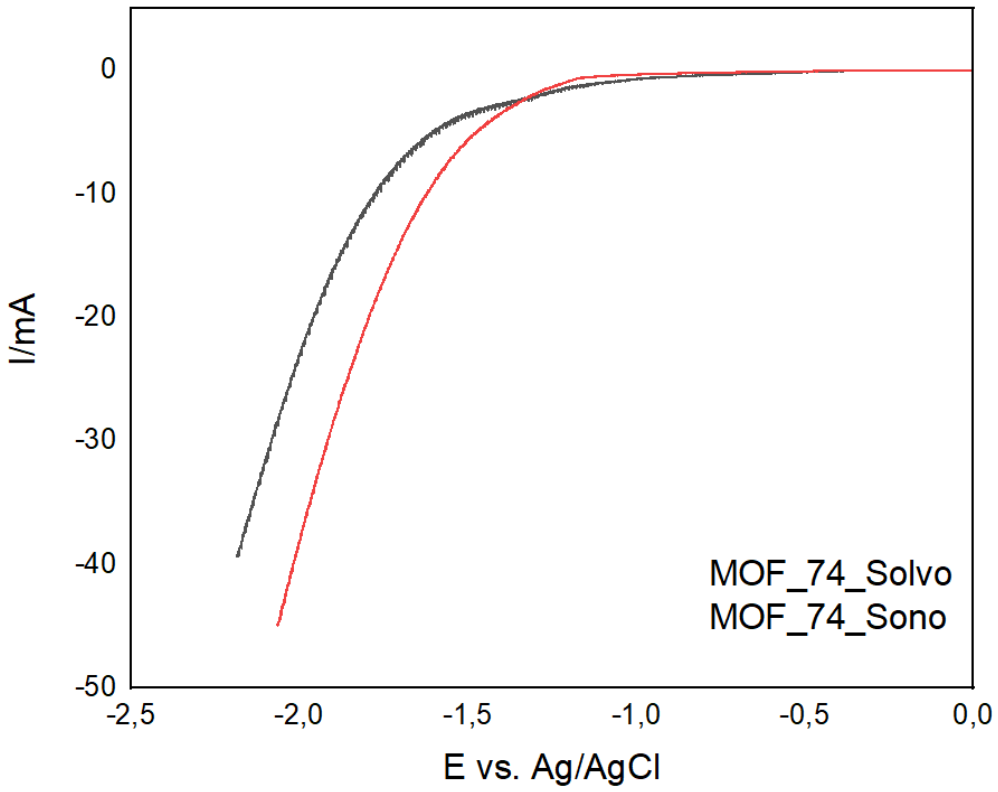

Figure 44: LSVs for MOF-74, US and ST (Black-ST; Red-US). At -2V MOF-74 US reaches its lowest current value -45mA – MOF-74 ST reaches -40mA at -2.2V

The interesting thing about the chronoamperometries is that the sonochemical sample is stable throughout the conduction of all measurements, as shown in Figure 39. As illustrated in Figure 38, MOF-74_ST drops current at -1.7V at 22 min. the current continues to drop at both -1.8V and -1.9V for the solvothermal sample. At -1.9V both materials start at 30mA, but the solvothermal reaches up to 42mA at the end of the measurement.

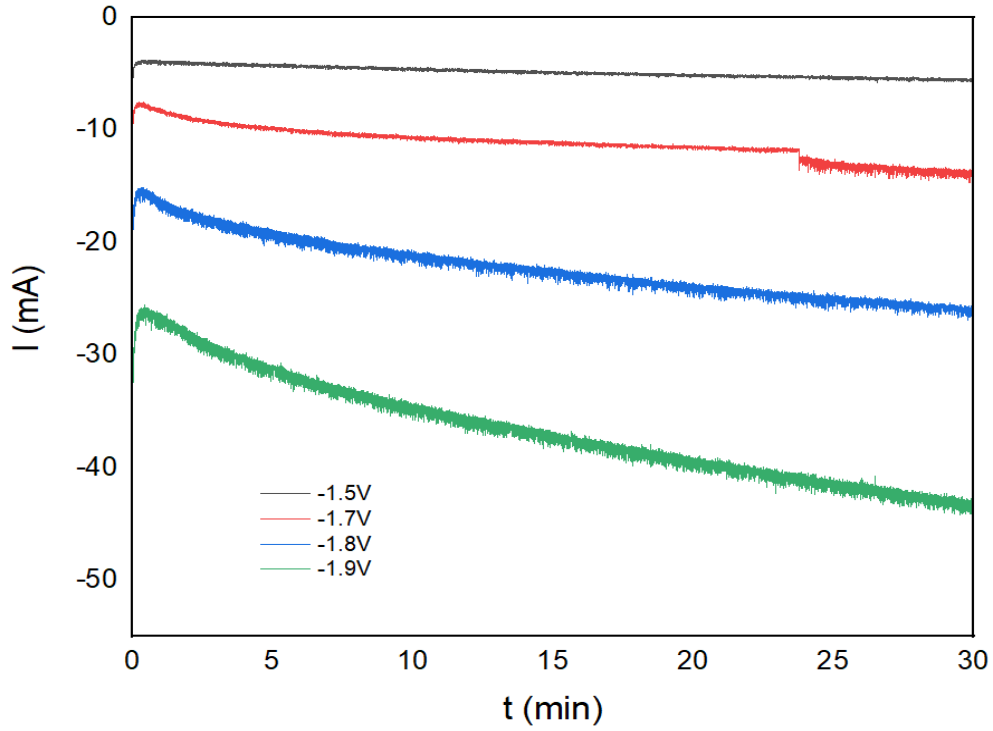

Figure 45: CA result for the solvothermal MOF-74 at different potentials

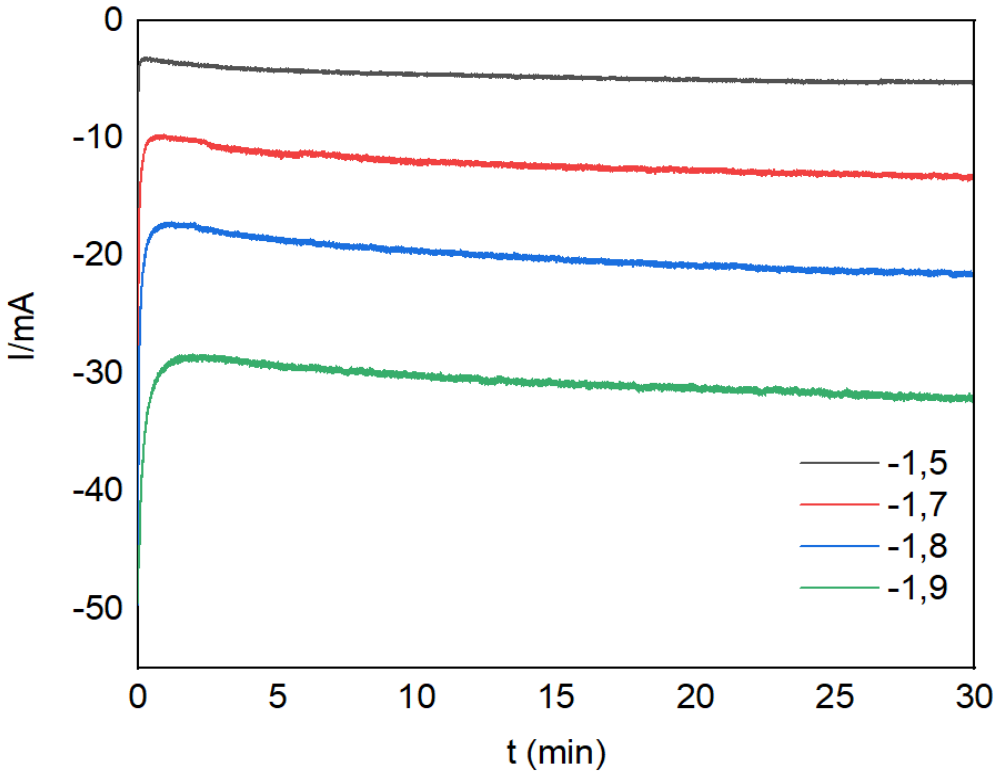

Figure 46: CA result for the sonochemical MOF-74 at different potentials

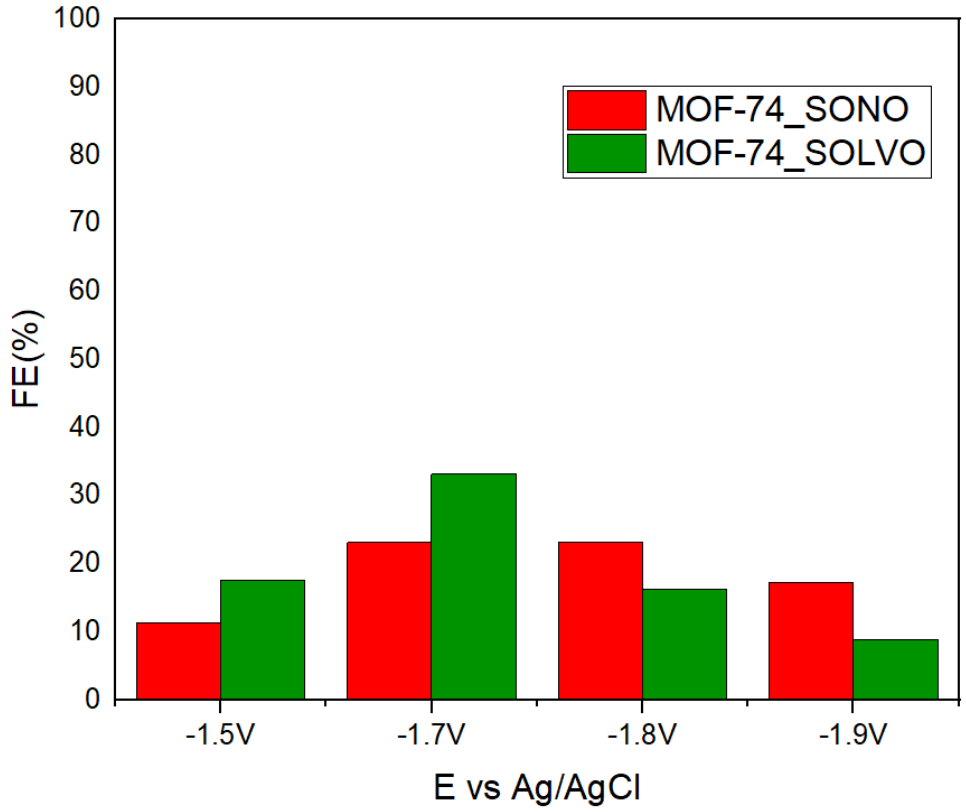

Figure 47: FE (%) for the MOF-74 US and ST. The sonochemical sample in red presents lower FE compared to the solvothermal in lower potentials

As far as the FE is concerned, even though it is observed that the solvothermal sample does not exhibit stability in the overall CAs, its performance in CO formation is far better. Its FE reaches up to 40% FE at -1.7V, almost doubling the efficiency from the measurement at -1.5V. On the contrary, the MOF-74_US illustrated lower FE, yet stable at -1.7V and -1.8V. On the contrary, its FE value at -1.9V exceeds the respective solvothermal

ZIF-8

The ZIF-8 are represented in two sections: one for the ZIF-8 fabricated with the three before mentioned pathways, and another one for the derived ZIF-8 at 500C compared to the zinc oxide.

The LSV measurement of the three ZIF-8 samples is illustrated in Figure 41. Room temperature fabricated and solvothermal are almost identical, while the sonochemical starts to drop current at -1.5V.

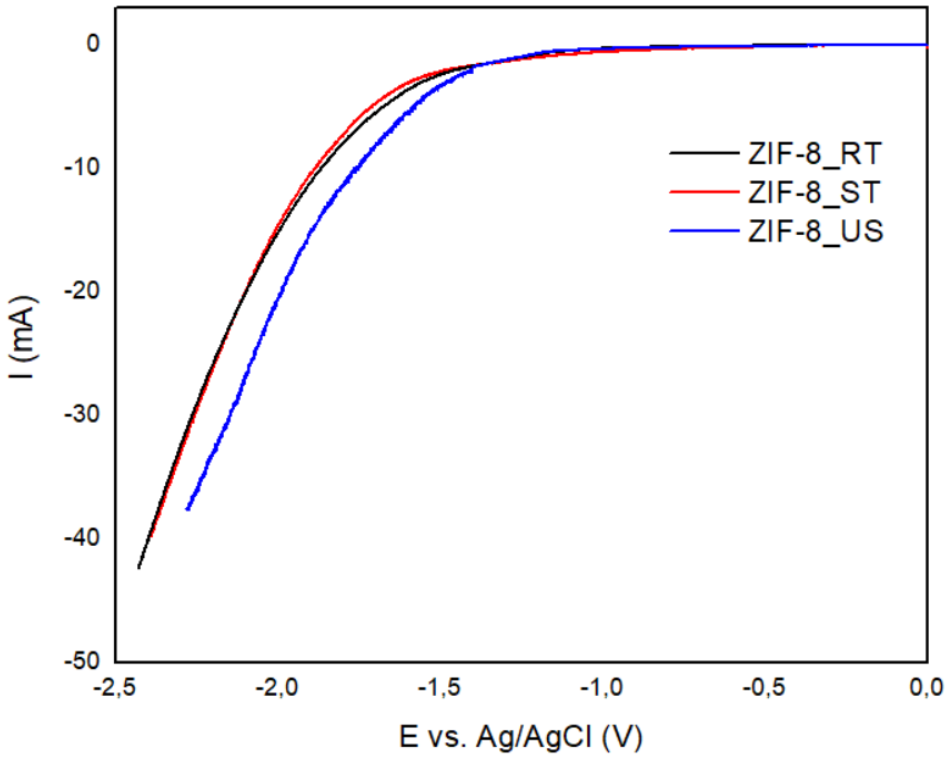

Figure 48: LSVs for the room temperature synthesized (black), solvothermal(red) and sonochemical ZIF-8 (blue)

Firstly, it is observed that the room temperature synthesized ZIF-8 reaches the potential of -2.2V without overloading, while the other two, solvothermal and sonochemical, reach -2V and -1.9V respectively. ZIF-8_RT seems to have the most stable behavior during all measurements, while solvothermal at -1.9V and -2V drops its current value. The sonochemical sample seems to keep stable current, but overloads at -25mA at -1.9V, while the RT sample reaches up to 33mA average at -2.2V. Another observation, regarding the solvothermal sample, is that between -1.9V and -2V the current drops almost half from -18mA to -32mA average.

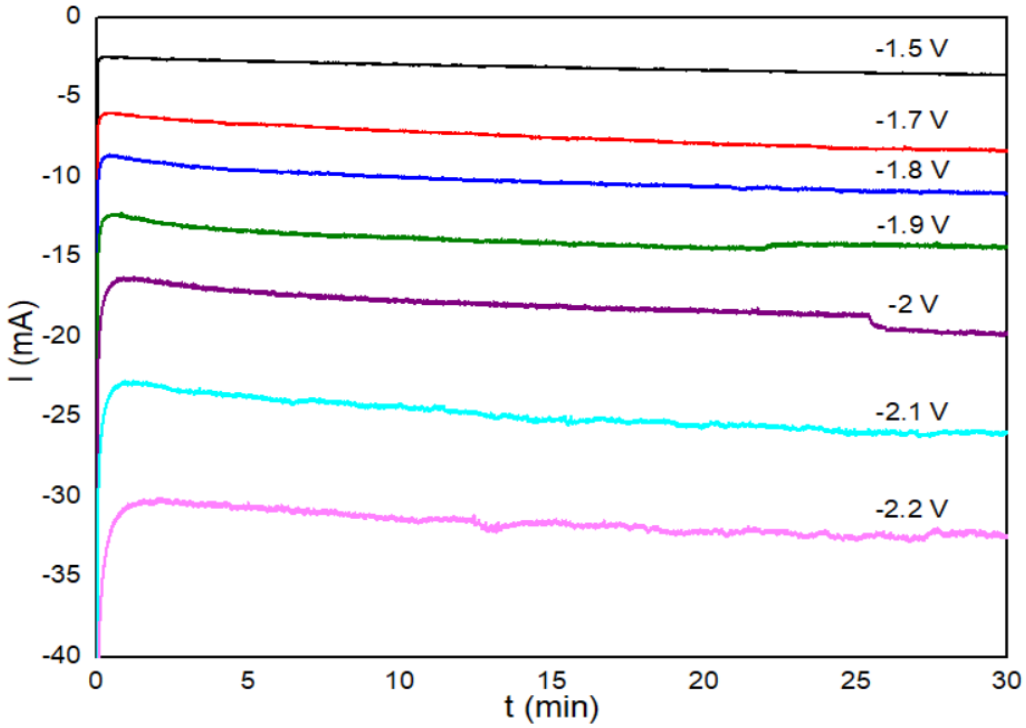

Figure 49: CA result for ZIF-8 RT in different potentials. It reaches -2.2V with -33mA average current

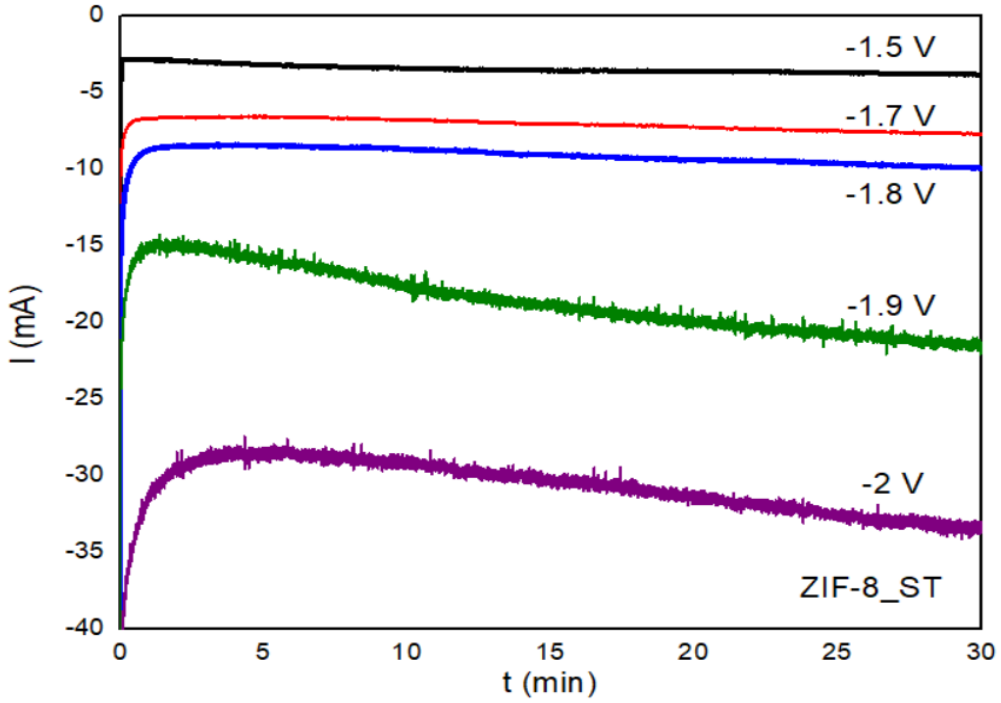

Figure 50: CA result for solvothermally synthesized ZIF-8. Current drops abruptly at -1.9V and -2V

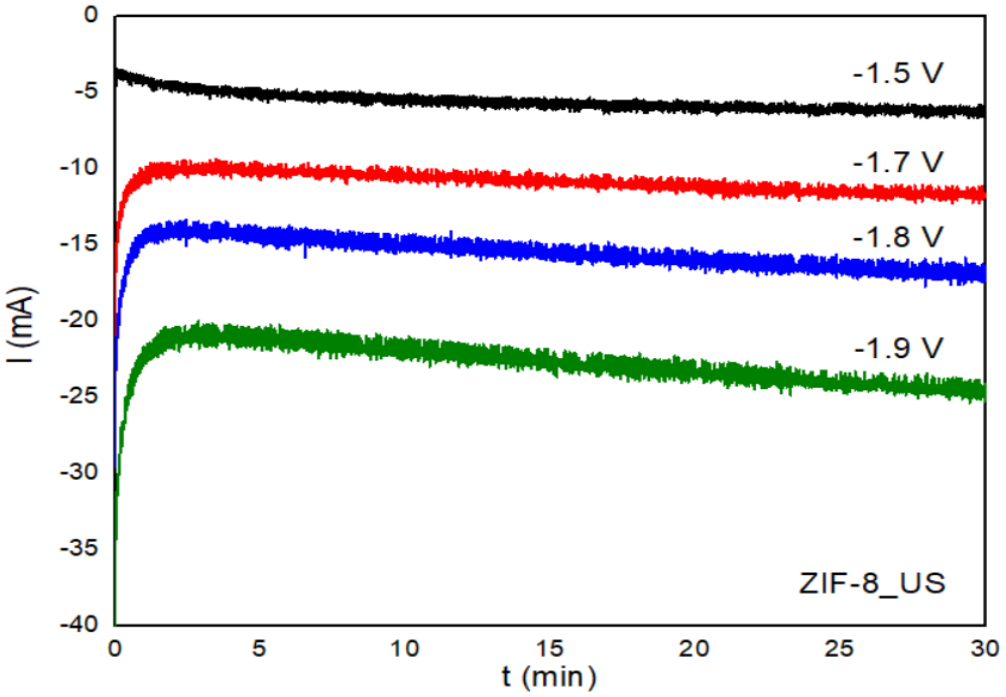

Figure 51: CA result for the sonochemical ZIF-8 in different potentials

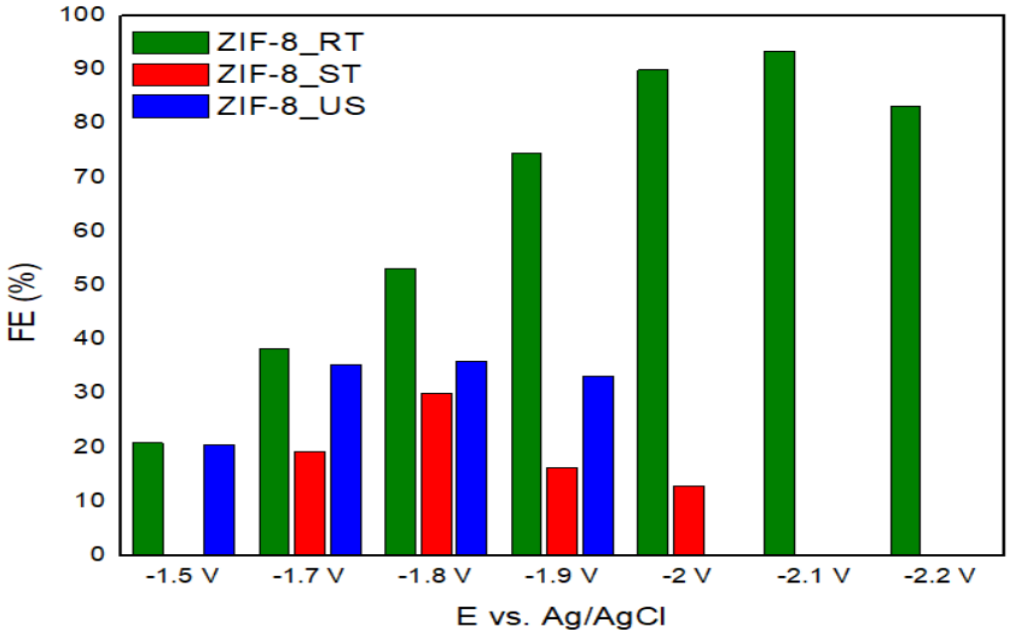

Figure 52: FE(%) of ZIF series. ZIF-8 RT(green) presents excellent FE up to 90% at -2.1V

As far as the FE is concerned, the best electrocatalytic behavior is presented by the room temperature synthesized ZIF-8. At -2.1V it reaches its highest value of 90%, while the rest of the samples reach up to 35% average, as shown in Figure 45. Moreover, the solvothermal

sample, does not result in product formation at -1.5V, reaches a high value of 33% and then drops until overloading. The sonochemical sample starts with the same FE values with the RT one at -1.5V and remains stable around 30% average until overloading.

The next experiments refer to the zinc oxide derived from the ZIF-8_RT after calcination at 500C, compared to a commercial zinc oxide. From 0V to -1.8V they seem identical, but afterwards the calcinated sample differs in slope and reaches -2.2V at -47mA, while the commercial reaches -2V at -40 mA, as illustrated in Figure 46.

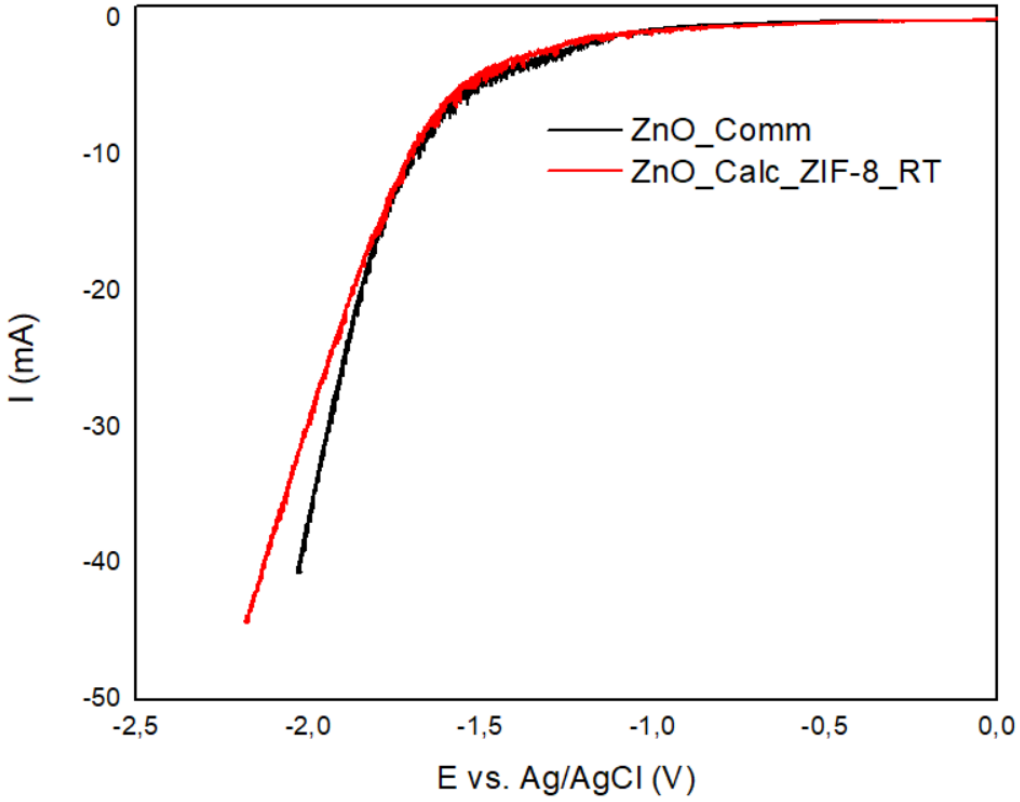

Figure 53: LSV of the commercial ZnO (black) and the derived from ZIF-8_RT (red). The last reaches up to -2.2V with -40mA, while the commercial -2V at -40mA

First and foremost, the commercial sample overloads at -1.9V terminating the measurement at 17min, as Figure 47 presents. Moreover, its potential reaches fully -1.8V, while the derived one reaches up to -2V without overloading, as seen in Figure 48. The derived sample appears more stable regarding current. At -1.8V the commercial ZnO has an average current value of 24 mA, while at the same potential the calcinated sample has an average value of -15 mA.

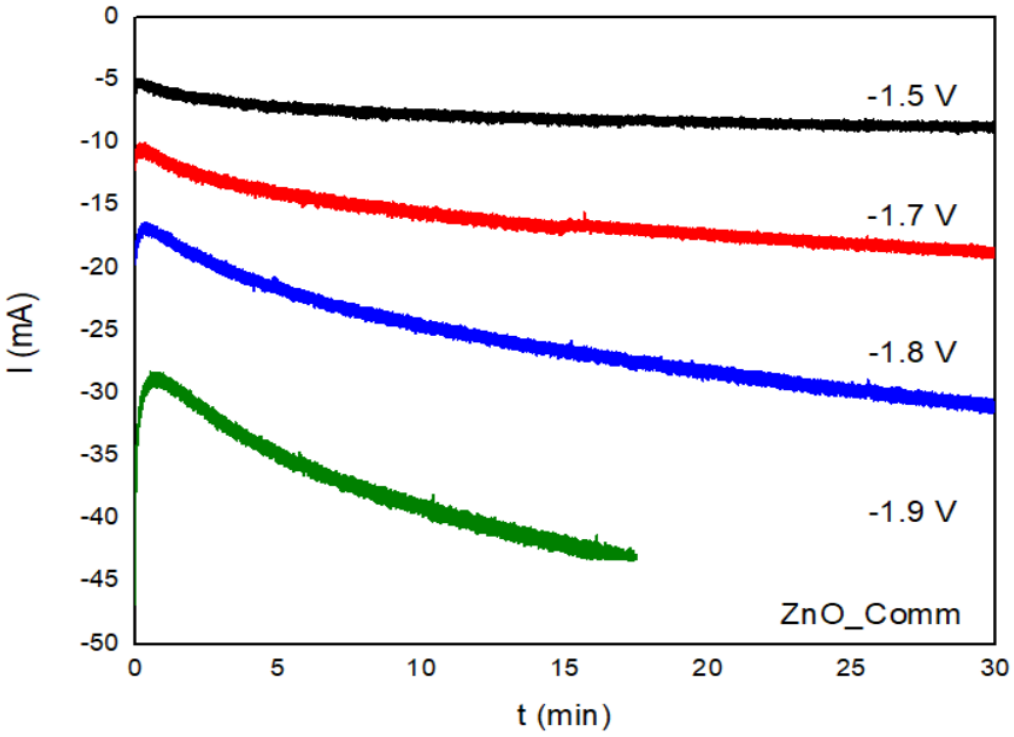

Figure 54: CA results for the commercial ZnO at different potential. At -1.9V the measurement is terminated at 17min due to electrode overloading

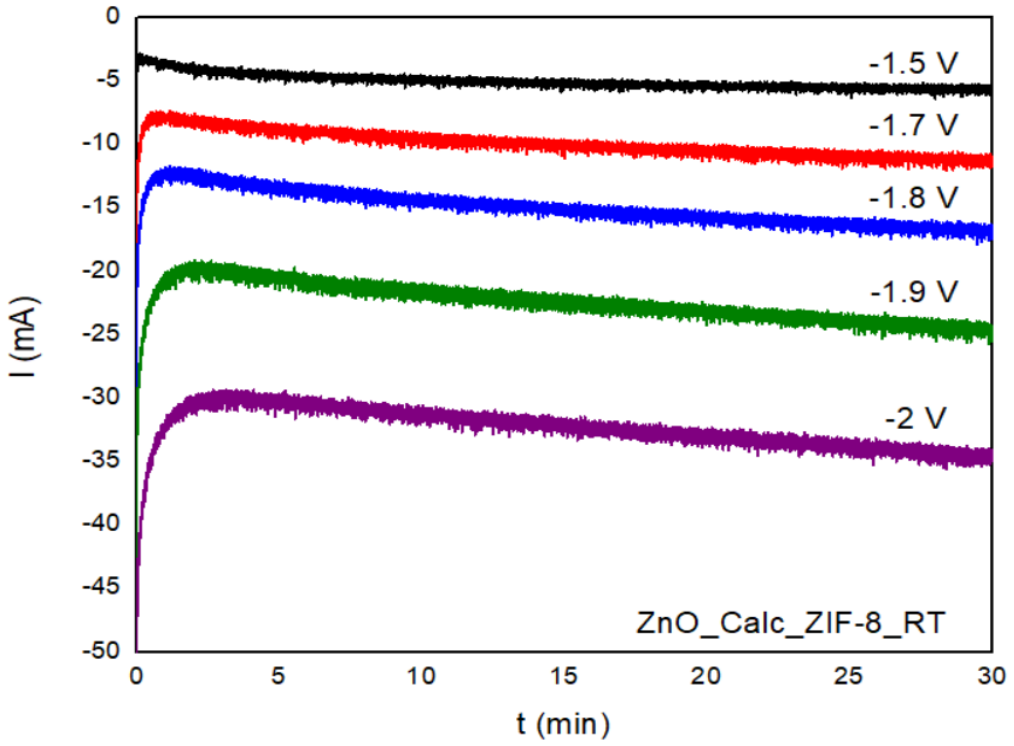

Figure 55: CA results for the derived from ZIF-8_RT ZnO at different potentials

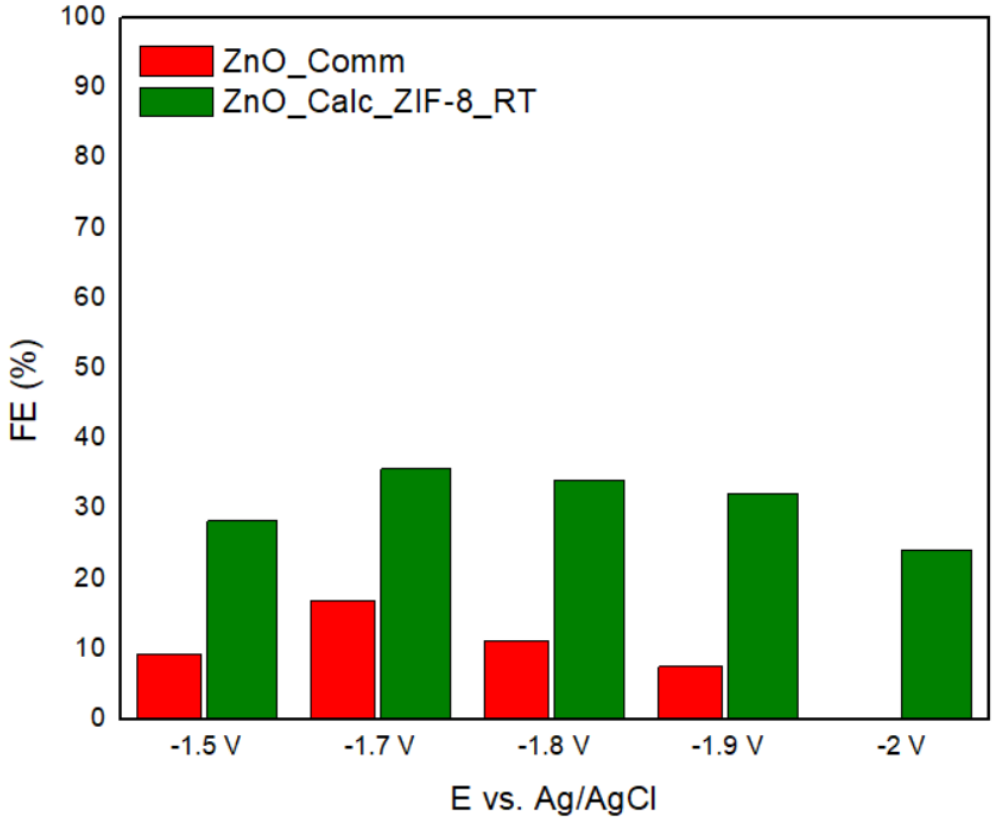

Figure 56: FE (%) comparison among commercial (red) and derived ZnO from ZIF-8 RT (green)

It is quite obvious from the chronoamperometries (Figures 47-48) that the calcinated sample reaches higher FE due to lower current values. Both, though, lead to product formation with the commercial ZnO having its highest value at 18%, while the derived ZnO reaches 33% at -1.7V, value that remains stable up to -1.9V, as Figure 49 represents.

5. Discussion

The results of the two parts of this thesis are discussed in this section. Firstly, some comments regarding the synthesis experiments are presented followed by results from the electrocatalytic ones, with an effort to reach a conclusion regarding tested MOFs catalytic behavior in CO2RR.

Regarding the synthesis experiments, three different synthesis methods are tested; the traditional solvothermal method, the room temperature with magnetic stirring and the sonochemical. For the copper series, there have been fabricated two sample of HKUST-1 via ultrasound and solvothermally, and one composite, the Cu/PANI MOF. All three were fabricated with one-to one molar ratio of the reactants yet in different volume ratios. The Ni series involve the Ni-BTC and two samples fabricated solvothermally and sonochemically for nickel and two linkers: BTC and Bipyridine. The last two were synthesized with the exact same quantities of precursors and solvents. The same value applied for the two samples of MOF-808. Finally, the zinc series include all three aforementioned synthesis methods. It is important to mention here, that some of the fabrications are based on literature, with the appropriate adjustments were needed. However, some sonochemical samples, such as the Ni-BTC/bpy are sonochemically synthesized for the first time.

The characterization method used for structure identification was X Ray Diffraction. Scanning Electron Microscopy was used for the observation of the size and the shape of the crystals.

As far as XRD is concerned, the HKUST-1 samples have been successfully synthesized, their XRD patterns are in accordance with the simulated. Cu/PANI MOF appears to display the same peaks as the simulated, so it is assumed that has been a successful experiment in terms of structure. The Ni-BTC MOF was also synthesized, but the obtained simulation XRD pattern from the CCDC is not in accordance with the experimental. This result may be due to many factors, such as not enough time in the convection oven to achieve crystallinity or maybe low temperature. The MOFs with nickel as the metal and the two linkers, BTC and bpy, present the same peaks with the simulated material.

MOF-808 samples were successfully fabricated according to XRD, even the sonochemical one. As far as the Zinc series are concerned, the MOF-74 samples are in accordance with literature, presenting the same peaks. The ZIF-8 experiments were successful, too. Finally, the ZnO derived from the ZIF-8_RT and the commercial ZnO are in accordance.

Regarding the SEM analysis, both the HKUST-1 fabricated MOFs do not present uniformity neither in size, nor in shape. In average, the sonochemical sample illustrates smaller crystals than the solvothermal. There is no uniformity in size and shape of the solvothermally prepared Ni-BTC/bpy, too. On the other hand, though, the sonochemically fabricated Ni-BTC/bpy presents clear size homogeneity, with smaller crystals than the solvothermal Ni-BTC/bpy. The solvothermal MOF-808 presents uniformity in size and shape with tetrahedral crystals, while the sonochemically prepared MOF-808 illustrates inhomogeneity.

As far as the sonochemical sample of MOF-74 is concerned, there is apparently uniformity in shape with rod-like crystals, but there is no uniformity is size. Among the ZIF-8 samples, the one fabricated in room temperature there are aggregates, but there is uniformity in size and shape with polyhedral crystals. The sonochemical ZIF-8 also presents crystals, with almost half the size of the ZIF-8_RT. The solvothermal ZIF-8, creates aggregates and sheet-like crystals with no uniformity in size and shape. This could possibly mean that there have been mistakes due to human factor during the synthesis, since this MOF has been studied thoroughly.

The second part involves the CO_2 Electroreduction experiments. Chronoamperometry and gas chromatography assisted these experiments in order to evaluate the catalytic behavior of the as synthesized MOFs in CO2RR via the calculation of faradaic efficiency.

Starting by the copper series, it was not possible to present the sonochemical HKUST-1 since it was tested twice in the lab without product formation. On the other hand, HKUST-1_ST and Cu/PANI were compared. The results are not quite as expected, mostly for HKUST-1, since it reached maximum 10% FE. Both electrodes collapsed at -1.8V at the end of the measurement. Cu/PANI MOF presented higher current than the HKUST-1 and did not lead to the formation of a higher quantity of carbon monoxide.

For the MOF-74 series the results differ, since the solvothermal sample reached up to 40%, while the sonochemical almost made it up to 5% at the same potential. This observation needs further investigation. Moreover, the sonochemical sample collapsed in lower current values than the solvothermal. One possible explanation might be the difference in conductivity, but yet again, there is the need of further analysis regarding the electrochemical activity.

Finally, in the ZIF-8 series, the room temperature synthesized MOF resulted in the highest values of faradaic efficiency among all rest of samples, 90%. It also, maintained this efficiency up to -2.2V, while the rest of the samples, the solvothermal and the sonochemical, collapsed and presented much lower values of faradaic efficiency. It is though quite interesting, that

even the sonochemical sample collapsed earlier, it maintained an average value of 30% FE from -1.5V to its overloading, while the solvothermal led to much lower of FE values. This is explained by the SEM experiment, since the solvothermal ZIF-8 did not appear uniform. The zinc oxides experiments lead to the observation, that the derived ZIF-8 presented much better efficiency than the commercial one, which remained stable up to -2V, while the commercial overloaded at -1.9V.

A general comment that should be done here is the method of deposition on the substrate. The deposition needs to be uniform and more accurate, such as via dipping.

6. Suggestions for Further Investigation

First of all, regarding CO2RR, more parameters should be investigated, such as the pH and the electrolyte effects. Moreover, the kinetics of the reaction must be thoroughly studied in order to have a better understanding of the simultaneous reaction, such as HER.

Moreover, this thesis approved that these certain MOFs lead to the formation of carbon monoxide. Regarding the condition the electrocatalytic experiment is conducted, the formation of other products should be investigated. The change of substrate, such as nickel or copper, to other than carbon might lead to different products.

As far as the synthesis is concerned, the major question is efficiency of the sonochemical route. For some MOFs, it led indeed to the formation of crystals that were identified as MOFs, but further investigation is needed for the optimization of the reaction conditions. It is quite an innovative method of material fabrication that could possibly lead to less reaction times.

Combining these two chapters now, one major conclusion of this thesis is that the material synthesis plays a huge role in their catalytic behavior. More comparisons should be done among MOFs regarding the synthesis paths. Characterization methods regarding the surface area of MOFs are highly recommended for the application of CO2RR.

Last but not least, it is recommended to expand MOFs potentials on bimetallics and oxides, and check their efficiency in CO2RR, since metals and oxides are commonly known as very good catalysts for this reaction.

References

1. Liao PQ, Shen JQ, Zhang JP. Metal–organic frameworks for electrocatalysis. *Coordination Chemistry Reviews*. 2018;373:22-48. doi:10.1016/j.ccr.2017.09.001

2. Wu YQ, Xie LH, Qin X, Sun YX, Xie YB, Li JR. Continuous crystalline membranes of a Ni(II)-based pillared-layer metal-organic framework in situ grown on nickel foam with two orientations. *Crystals (Basel)*. 2018;8(10). doi:10.3390/cryst8100383

3. Rowsell JLC, Yaghi OM. Metal-organic frameworks: A new class of porous materials. *Microporous and Mesoporous Materials*. 2004;73(1-2):3-14. doi:10.1016/j.micromeso.2004.03.034

4. Kuppler RJ, Timmons DJ, Fang QR, et al. Potential applications of metal-organic frameworks. *Coordination Chemistry Reviews*. 2009;253(23-24):3042-3066. doi:10.1016/j.ccr.2009.05.019

5. Lee J, Farha OK, Roberts J, Scheidt KA, Nguyen ST, Hupp JT. Metal-organic framework materials as catalysts. *Chemical Society Reviews*. 2009;38(5):1450-1459. doi:10.1039/b807080f

6. Synthesis, characterisation and properties of new metal-organic frameworks.

7. Cheyne RM, W Jones CH, Wilson RM, et al. *International Tables for X-Ray Crystallography*. Vol 16. Kynoch Press; 1977.

8. Bartoll J. *For the Very First Time a Large Collection of French 18th Century Paintings by Antoine Watteau and His Circle Has Been Studied in Detail*. www.ndt.net/search/docs.php3?MainSource=65

9. Cook TR, Zheng YR, Stang PJ. Metal-organic frameworks and self-assembled supramolecular coordination complexes: Comparing and contrasting the design, synthesis, and functionality of metal-organic materials. *Chemical Reviews*. 2013;113(1):734-777. doi:10.1021/cr3002824

10. Verbindungen von Kohlenwasserstoffen mit Metallsalzen.

11. Dyadin YA, Terekhova IS, Rodionova T v., Soldatov D v. Half-century history of clathrate chemistry. *Journal of Structural Chemistry*. 1999;40(5):645-653. doi:10.1007/BF02903441

12. Yaghi, Omar M._Kalmutzki, Markus J._Diercks, Christian S._ & Markus J. Kalmutzki & Christian S. Diercks - Introduction to Reticular Chemistry-John Wiley & Sons, Inc. (2019).

13. ~l B }~qo :, De C:~!, Yves P, Athey ~ [, Nazi~res C, Setton R. *FOP~iATION OF 3-DI~NSIONAL STRUCTURES USING BIFSq~CT!OH,TL L!GA~D BRIDGES*. Vol 13. Pergamon Press; 1977.

14. Walker GF, Hawthorne DG. *Complexes Between N-Alkylamines and Nickel Cyanide*.; 1967.

15. Iwamoto T, Miyoshi T, Miyamoto T, Sasaki Y, Fujiwara S. *The Metal Ammine Cyanide Aromatics Clathrates. I. The Prepara-Tion and Stoichiometry of the Diamminemetal(II) Tetracyano-Niccolate(II) Dibenzene and Dianiline*1*. Vol 40.; 1967.

16. A. F. Wells, The geometrical basis of crystal chemistry. Part 1, Acta Crystallogr., 7 ,1954, 535–544.

17. Hoskins BF, Robson R. *Design and Construction of a New Class of Scaffolding-like Materials Comprising Infinite Polymeric Frameworks of 3D-Linked Molecular Rods. A Reappraisal of the Zn(CN)2 and Cd(CN)2 Structures and the Synthesis and Structure of the Diamond-Related Frameworks [N(CH3)4][CuIZnII(CN)4] and CuI[4,4/,4//,4///-Tetracyanotetraphenylmethane]BF4*xC6H5N02*. Vol 112.; 1990. https://pubs.acs.org/sharingguidelines

18. *Communications to the Editor*.

19. Fujita, M., Yazaki, J., & Ogura, K. (1990). Preparation of a macrocyclic polynuclear complex, [(en)Pd(4,4'-bpy)]4(NO3)8 (en = ethylenediamine, bpy = bipyridine), which recognizes an orga.

20. Fujita M, Yoon Jung Kwon st, Washizu S, Ogura K. *Preparation, Clathration Ability, and Catalysis of a Two-Dimensional Square Network Material Composed of Cadmium(11) and 4,Y-Bipyridine*. Vol 116.; 1994.

21. Yaghi . M, Li H. *Hydrothermal Synthesis of a Metal-Organic Framework Containing Large Rectangular Channels*. Vol 117.; 1995.

22. Yaghi, O. M., Li, G., & Li, H. (1995). Selective binding and removal of guests in a microporous metal–organic framework. Nature, 378(6558), 703–706.

23. Li, H., Eddaoudi, M., O'Keeffe, M., & Yaghi, O. M. (1999). Design and synthesis of an exceptionally stable and highly porous metal-organic framework. Nature, 402(6759), 276–279.

24. Synthesis, characterisation and properties of new metal-organic frameworks.

25. Furukawa H, Cordova KE, O'Keeffe M, Yaghi OM. The chemistry and applications of metal-organic frameworks. *Science (1979)*. 2013;341(6149). doi:10.1126/science.1230444

26. Daglar H, Keskin S. Recent advances, opportunities, and challenges in high-throughput computational screening of MOFs for gas separations. *Coordination Chemistry Reviews*. 2020;422. doi:10.1016/j.ccr.2020.213470

27. Batten SR, Champness NR, Chen XM, et al. Terminology of metal-organic frameworks and coordination polymers (IUPAC recommendations 2013). *Pure and Applied Chemistry*. 2013;85(8):1715-1724. doi:10.1351/PAC-REC-12-11-20

28. Vaitsis C, Sourkouni G, Argirusis C. Metal Organic Frameworks (MOFs) and ultrasound: A review. *Ultrasonics Sonochemistry*. 2019;52:106-119. doi:10.1016/j.ultsonch.2018.11.004

29. Stock N, Biswas S. Synthesis of metal-organic frameworks (MOFs): Routes to various MOF topologies, morphologies, and composites. *Chemical Reviews*. 2012;112(2):933-969. doi:10.1021/cr200304e

30. Butova V v, Soldatov MA, Guda AA, Lomachenko KA, Lamberti C. Metal-organic frameworks: structure, properties, methods of synthesis and characterization. *Russian Chemical Reviews*. 2016;85(3):280-307. doi:10.1070/rcr4554

31. Rabenau A. *The Role of Hydrothermal Synthesis in Preparative Chemistry*.

32. Stock N, Biswas S. Synthesis of metal-organic frameworks (MOFs): Routes to various MOF topologies, morphologies, and composites. *Chemical Reviews*. 2012;112(2):933-969. doi:10.1021/cr200304e

33. Butova V v, Soldatov MA, Guda AA, Lomachenko KA, Lamberti C. Metal-organic frameworks: structure, properties, methods of synthesis and characterization. *Russian Chemical Reviews*. 2016;85(3):280-307. doi:10.1070/rcr4554

34. Bian Y, Xiong N, Zhu G. Technology for the remediation of water pollution: A review on the fabrication of metal organic frameworks. *Processes*. 2018;6(8). doi:10.3390/pr6080122

35. Zhang H. *The History of Microwave Heating Transform Into A Flameless Civilization View Project Energy Use and Climate Changes View Project*.; 2017. https://www.researchgate.net/publication/312192693

36. Rubio-Martinez, M., Avci-Camur, C., Thornton, A. W., Imaz, I., Maspoch, D., & Hill, M. R. (2017). New synthetic routes towards MOF production at scale. Chemical Society Reviews, 46(11), 3453–3480.

37. Ni Z, Masel RI. Rapid production of metal-organic frameworks via microwave-assisted solvothermal synthesis. *J Am Chem Soc*. 2006;128(38):12394-12395. doi:10.1021/ja0635231

38. Lee YR, Kim J, Ahn WS. Synthesis of metal-organic frameworks: A mini review. *Korean Journal of Chemical Engineering*. 2013;30(9):1667-1680. doi:10.1007/s11814-013-0140-6

39. Tehrani AA, Safarifard V, Morsali A, Bruno G, Rudbari HA. Ultrasound-assisted synthesis of metal-organic framework nanorods of Zn-HKUST-1 and their templating effects for facile fabrication of zinc oxide nanorods via solid-state transformation. *Inorganic Chemistry Communications*. 2015;59:41-45. doi:10.1016/j.inoche.2015.06.028

40. Mueller, U.; Puetter, H.; Hesse, M.; Wessel, H. WO 2005/ 049892.

41. M. Taddei, D. A. Steitz, J. A. van Bokhoven and M. Ranocchiari, Continuous-Flow Microwave Synthesis of Metal–Organic Frameworks: A Highly Efficient Method for Large-Scale Production, Chem. – Eur. J., 2016, 22, 3245–3249.

42. H. Al-Kutubi, J. Gascon, E. J. R. Sudho¨lter and L. Rassaei, Electrosynthesis of Metal–Organic Frameworks: Challenges and Opportunities, ChemElectroChem, 2015, 2, 462–474.

43. M. Dincaˇ and M. Li, Methods for electrochemically induced cathodic deposition of crystalline metal–organic frameworks, 2014.

44. Schlesinger, M.; Schulze, S.; Hietschold, M.; Mehring, M. Microporous Mesoporous Mater. 2010, 132, 121.

45. T. Friskin´, Supramolecular concepts and new techniques in mechanochemistry: cocrystals, cages, rotaxanes, open metal–organic frameworks, Chem. Soc. Rev., 2012, 41, 3493–3510.

46. G. Kaupp, Solid-state molecular syntheses: complete reactions without auxiliaries based on the new solid-state mechanism, CrystEngComm, 2003, 5, 117–133.

47. A. L. Garay, A. Pichon and S. L. James, Solvent-free synthesis of metal complexes, Chem. Soc. Rev., 2007, 36, 846–855.

48. A. Stolle, T. Szuppa, S. E. S. Leonhardt and B. Ondruschka, Ball milling in organic synthesis: solutions and challenges, Chem. Soc. Rev., 2011, 40, 2317–2329.

49. V. V. Boldyrev, Mechanochemistry and mechanical activation of solids, Solid State Ionics, 1993, 63, 537–543.

50. D. E. Crawford and J. Casaban, Recent Developments in Mechanochemical Materials Synthesis by Extrusion, Adv. Mater., 2016, 28, 5747–5754.

51. S. L. James, et al., Mechanochemistry: opportunities for new and cleaner synthesis, Chem. Soc. Rev., 2012, 41, 413–447.

52. Chen, D., Zhao, J., Zhang, P., & Dai, S. (2019). Mechanochemical Synthesis of Metal-organic Frameworks. Polyhedron.

53. Thrush A, Martin K, Hoskins PR (eds) (2010) Diagnostic ultrasound. Cambridge University Press, UK.

54. Pollet BG, Ashokkumar M. *SPRINGER BRIEFS IN MOLECULAR SCIENCE ULTRASOUND AND SONOCHEMISTRY*. http://www.springer.com/

55. Gallego-Juarez JA, Graff KF (eds) (2017) Power ultrasonics: applications of high-intensity ultrasound. Elsevier Science and Technology, UK.

56. Ashokkumar M, Cavalieri F, Chemat F, Okitsu K, Sambandam A, Yasui K, Zisu B (eds) (2016) Handbook of ultrasonics and sonochemistry, vol 1 and 2. Springer Reference, Singapore.

57. Chen D, Sharma SK, Mudhoo A (eds) (2012) Handbook on applications of ultrasound: sonochemistry for sustainability. CRC Press, USA.

58. Feng H, Weiss J, Barbosa-Cánovas G (eds) (2011) Ultrasound technologies for food and bioprocessing. Springer, New York.

59. Xu, Hangxun & Zeiger, Brad & Suslick, Kenneth. (2012). Sonochemical Synthesis of Nanomaterials. Chemical Society reviews. 42.

60. Ashokkumar M, Mason T (2007) Sonochemistry, Kirk-Othmer encyclopedia of chemical technology. Wiley, USA.

61. S Pearsall Cavitation (London: Mills and Boon, 1972).

62. Bowen Cai, Janine Mazahreh, Qingyu Ma, Fang Wang, Xiao Hu, Ultrasound-assisted fabrication of biopolymer materials: A review, International Journal of Biological Macromolecules, Volume 209, Part B, 2022, Pages 1613-1628.

63. L-G Qiu, Z-Q Li, Y Wu, W Wang, T Xu, X Jiang Chem. Commun. 3642 (2008).

64. W-J Son, Jun Kim, Jah Kim, W-S Ahn Chem. Commun. 6336 (2008).

65. Z-Q Li, L-G Qiu, T Xu, Y Wu,W Wang, Z-Y Wu, X Jiang Mater. Lett. 63 78 (2009).

66. M Schlesinger, S Schulze, M Hietschold, M Mehring Microporous Mesoporous Mater. 132 121 (2010).

67. Xu, F.; Xian, S.; Xia, Q.; Li, Y.; Li, Z., Effect of Textural Properties on the Adsorption and Desorption of Toluene on the Metal-Organic Frameworks HKUST-1 and MIL-101. Adsorption Science Technology 2013, 31 (4), 325-340.

68. Yoon, M.; Srirambalaji, R.; Kim, K., Homochiral metal-organic frameworks for asymmetric heterogeneous catalysis. Chemical reviews 2012, 112 (2), 1196- 231.

69. Li, J. R.; Sculley, J.; Zhou, H. C., Metal-organic frameworks for separations. Chemical reviews 2012, 112 (2), 869-932.

70. Nations U, of Economic D, Affairs S, Division P. *World Population Prospects 2019 Highlights*.

71. IEO2021_ReleasePresentation.

72. https://mahb.stanford.edu/library-item/fossil-fuels-run/.

73. IEA, Total primary energy supply by fuel, 1971 and 2019, IEA, Paris https://www.iea.org/data-and-statistics/charts/total-primary-energy-supply-by-fuel-1971-and-2019.

74. https://www.eia.gov/.

75. Contribution of Working Group I to the Fifth Assessment Report of the Intergovernmental Panel on Climate Change. [Stocker, T. F., D. Qin, G.-K. Plattner, M. Tignor, S. K. Allen, J. Boschung, A. Nauels, Y. Xia, V. Bex and P. M. Midgley (eds.)]. Cambridge University Press, Cambridge, United Kingdom and New York, NY, USA, 1585 pp.

76. Draper AM, Weissburg MJ. Impacts of global warming and elevated CO2 on sensory behavior in predator-prey interactions: A review and synthesis. *Frontiers in Ecology and Evolution*. 2019;7(MAR). doi:10.3389/fevo.2019.00072

77. https://ourworldindata.org/co2-emissions.

78. Usman M, Humayun M, Garba MD, et al. Electrochemical reduction of co2: A review of cobalt based catalysts for carbon dioxide conversion to fuels. *Nanomaterials*. 2021;11(8). doi:10.3390/nano11082029

79. https://www.epa.gov/ghgemissions/global-greenhouse-gas-emissions-data.

80. https://www.climate.gov/news-features/understanding-climate/climate-change-atmospheric-carbon-dioxide.

81. https://www.climate.gov/news-features/understanding-climate/climate-change-atmospheric-carbon-dioxide.

82. Intergovernmental Panel on Climate Change, IPCC, http://www.ipcc.ch/index.html.

83. *UNITED NATIONS FRAMEWORK CONVENTION ON CLIMATE CHANGE*.

84. *KYOTO PROTOCOL TO THE UNITED NATIONS FRAMEWORK CONVENTION ON CLIMATE CHANGE UNITED NATIONS*.; 1998.

85. Unfccc. *ADOPTION OF THE PARIS AGREEMENT - Paris Agreement Text English*.

86. Usman M, Humayun M, Garba MD, et al. Electrochemical reduction of co2: A review of cobalt based catalysts for carbon dioxide conversion to fuels. *Nanomaterials*. 2021;11(8). doi:10.3390/nano11082029

87. D.A. Lowy, M. Jitaru, in: Kwong-Yu Chan, Chi-Ying, V. Li (Eds), Electrochemically Enabled Sustainability, Devices, Materials and Mechanisms for Energy Conversion, CRC Press, 2014.

88. Chan KY, Li CYV. *Electrochemically Enabled Sustainability: Devices, Materials and Mechanisms for Energy Conversion*.

89. Muradov, N.Z., & Veziroglu, T. (Eds.). (2011). Carbon-Neutral Fuels and Energy Carriers (1st ed.). CRC Press.

90. Beck J, Johnson R, Naya T. Electrochemical Conversion of Carbon Dioxide to Hydrocarbon Fuels EME 580 Spring 2010.

91. Albo J, Alvarez-Guerra M, Castaño P, Irabien A. Towards the electrochemical conversion of carbon dioxide into methanol. *Green Chemistry*. 2015;17(4):2304-2324. doi:10.1039/c4gc02453b

92. Liang, F., Zhang, K., Zhang, L., Zhang, Y., Lei, Y., Sun, X., Recent Development of Electrocatalytic CO2 Reduction Application to Energy Conversion. Small 2021, 17,

93. K.P. Kuhl, E.R. Cave, D.N. Abram, T.F. Jaramillo, New insights into the electrochemical reduction of carbon dioxide on metallic copper surfaces, Energy Environ. Sci., 5, 2012, 7050.

94. Samanta S, Srivastava R. Catalytic conversion of CO2to chemicals and fuels: The collective thermocatalytic/photocatalytic/electrocatalytic approach with graphitic carbon nitride. *Materials Advances*. 2020;1(6):1506-1545. doi:10.1039/d0ma00293c

95. Azizi O, Jafarian M, Gobal F, Heli H, Mahjani MG. The investigation of the kinetics and mechanism of hydrogen evolution reaction on tin. *International Journal of Hydrogen Energy*. 2007;32(12):1755-1761. doi:10.1016/j.ijhydene.2006.08.043

96. Quaino PM, Gennero de Chialvo MR, Chialvo AC. Hydrogen electrode reaction: A complete kinetic description. *Electrochimica Acta*. 2007;52(25):7396-7403. doi:10.1016/j.electacta.2007.06.030

97. M.R.Gennero de Chialvo, A.C. Chialvo, Hydrogen evolution reaction: Analysis of the Volmer-Heyrovsky-Tafel mechanism with a generalized adsorption model, Journal of Electroanalytical Chemistry, Volume 372, Issues 1–2,199498. P.M. Quaino, M.R. Gennero de Chialvo, A.C. Chialvo, Hydrogen electrode reaction: A complete kinetic description, Electrochimica Acta, 52(25), 2007, 7396.

99. Y. Hori, in: C. Vayenas (Ed.), Electrochemical CO2 reduction on metal electrodes, Modern Aspects of Electrochemistry, Springer, New York, 2008.

100. Alessandro Senocrate, Corsin Battaglia, Electrochemical CO2 reduction at room temperature: Status and perspectives, Journal of Energy Storage, Volume 36, 2021, 102373.

101. J.K. Nørskov, F. Studt, F. Abild-Pedersen, T. Bligaard Fundamental Concepts in Heterogeneous Catalysis John Wiley & Sons, Inc, Hoboken, NJ, USA (2014),.

102. Y.Y. Birdja, E. Pérez-Gallent, M.C. Figueiredo, A.J. Göttle, F. Calle-Vallejo, M.T.M. Koper Advances and challenges in understanding the electrocatalytic conversion of carbon dioxide to fuels.

103. Hinogami R, Yotsuhashi S, Deguchi M, Zenitani Y, Hashiba H, Yamada Y. Electrochemical reduction of carbon dioxide using a copper rubeanate metal organic framework. *ECS Electrochemistry Letters*. 2012;1(4). doi:10.1149/2.001204eel

104. Israr F, Kim DK, Kim Y, Oh SJ, Ng KC, Chun W. Synthesis of porous Cu-BTC with ultrasonic treatment: Effects of ultrasonic power and solvent condition. *Ultrasonics Sonochemistry*. 2016;29:186-193. doi:10.1016/j.ultsonch.2015.08.023

105. Neisi Z, Ansari-Asl Z, Dezfuli AS. Polyaniline/Cu(II) Metal-organic Frameworks Composite for High Performance Supercapacitor Electrode. *Journal of Inorganic and Organometallic Polymers and Materials*. 2019;29(6):1838-1847. doi:10.1007/s10904-019-01145-9

106. Nirmal, Sharma K, Poonam, Tripathi SK. Synthesis and characterization of Ni-BTC MOF for supercapacitor electrode. In: *AIP Conference Proceedings*. Vol 2265. American Institute of Physics Inc.; 2020. doi:10.1063/5.0017162

107. Furukawa H, Gándara F, Zhang YB, et al. Water adsorption in porous metal-organic frameworks and related materials. *J Am Chem Soc*. 2014;136(11):4369-4381. doi:10.1021/ja500330a

108. Lin R, Guo J, Li X, Patel P, Seifitokaldani A. Electrochemical reactors for CO2 conversion. *Catalysts*. 2020;10(5). doi:10.3390/catal10050473

109. Bontempelli, G., N. Dossi, and R. Toniolo, Linear Sweep and Cyclic, in Reference Module in Chemistry, Molecular Sciences and Chemical Engineering. 2016, Elsevier.

110. *Britannica, T. Editors of Encyclopaedia (2021, March 25). Faraday's Laws of Electrolysis. Encyclopedia Britannica.*